

1 Nanofluid flow and heat transfer of carbon nanotube and graphene
2 platelette nanofluids in entrance region of microchannels

3 Mark E. Fuller^{a,*}, Joseph T. C. Liu^b

4 ^a*Physico-Chemical Fundamentals of Combustion, RWTH Aachen University, 52062 Aachen, Germany*

5 ^b*School of Engineering, Brown University, Providence, RI 02912, USA*

6 **Abstract**

Suspensions of nano-scale particles in liquids, dubbed nanofluids, are of great interest for heat transfer applications. Nanofluids potentially offer superior thermal conductivity to alternative, pure fluids and are of particular interest in applications where active cooling of power-dense systems is required. In this work, the thermophysical properties of carbon nanotube nanofluids (CNTNf) and those of graphene nanoplatelette nanofluids (GNPNf) as functions of particle volume fraction are deduced from published experiments. These properties are applied to a perturbative boundary layer model to examine how the velocity and temperature profiles (and correspondingly shear stress and surface heat transfer) vary with the nanoparticle concentration in the entrance region of microchannels. Findings of this modeling effort indicate that both shear stress and heat transfer in GNPNf increase with increasing particle concentration. The normalized increase in shear stress is approximately twice that for heat transfer as a function of GNP particle concentration. Interestingly, CNTNf shows anti-enhancement heat transfer behaviour; an increasing concentration of CNT nanoparticles is associated with both an increase in shear stress and a decrease in the surface heat transfer rate.

7 *Keywords:* Nanofluids, Heat Transfer, Carbon Nanotubes, Graphene Nanoplatelettes

*Corresponding author

8 1. Introduction

9 Since the pioneering work of Choi and Eastman [1], nanofluids have become widespread
10 in applications and stimulated much work on their fundamental understanding, *e.g.* [2–
11 10]. Our previous theoretical-numerical work [11–13] performed studies of nanofluids with
12 dispersed spherical metallic nanoparticles (alumina and gold) using a perturbation method
13 for small volume concentration. More recently, carbon nanotubes (CNT) and graphene
14 nanoplatelettes (GNP) have become subjects of intense studies because of their thermo-
15 physical properties, *e.g.* [14–32].

16 This paper applies the methodologies previously developed by the authors to nanofluids
17 consisting of multi-walled CNT (MWCNT) and GNP dispersed in liquid; we refer to these
18 nanofluid mixtures respectively as CNTnf and GNPNf. Both CNT and GNP are graphene
19 structures, based on two-dimensional arrays of carbon atoms. CNT are hollow cylinders
20 where the graphene sheet is “rolled up” either with the edges joined to form a continuous
21 cylinder (and therefore single-atom thick wall, “single-walled”, SWCNT) or in a spiral,
22 “scroll” structure [33, 34]. The term MWCNT refers to both multiple concentric single-
23 walled tubes and “scroll” spiral-form tubes where the sheet is wound such that it overlaps
24 itself. GNP, in contrast, consist of stacked or layered sheets of graphene where the layers
25 are held together with van der Waals forces [35]. The thermophysical properties of the
26 nanofluids that are required for this model and analysis are drawn from ref. 14 and ref. 36,
27 respectively. Application to the entrance region of microchannels is made, as measurements
28 in alumina nanofluids indicate that the largest nanofluid effect is in this region [37]. In
29 the entrance region of the channels, the boundary layer thickness is small compared to the
30 tube diameter and simplified modeling may be accomplished by considering the models of
31 boundary layers in flow over flat plates. Both momentum and thermal boundary layers for
32 flow over flat plates are solved problems in laminar flow owing to the respective works of
33 Blasius [38] and Pohlhausen [39].

34 A thorough overview of recent developments in the use of carbon-based nanofluids for
35 heat transfer and in heat exchangers is provided in ref. 27. Experimental determination of

36 the properties of nanofluid mixtures (discussed in greater detail in section 2) alone has been
37 the subject of multiple articles. While the totality of articles is too numerous to mention,
38 certain studies are worth recounting. Measurements of thermal conductivity of water-CNT
39 nanofluids [40] show variable enhancement depending on the exact morphology of the CNT
40 utilized, comparing SWCNT of small aspect ratios (“short”), large aspect ratios (“long”),
41 and MWCNT. In the study of ref. 40, the most enhancement is observed for the long
42 SWCNT and the least with MWCNT. The summary in ref. 27 also indicates that there
43 have been multiple reports of viscosity of MWCNT-water nanofluids decreasing relative to
44 the base fluid at low particle loadings (up to 0.2 vol%) and increasing thereafter [41–43].
45 For GNP, both viscosity and thermal conductivity were examined by Mehrali *et al.* [44] as a
46 function of the specific surface area of the GNP (300, 500, 750 m²/g). There, both thermal
47 conductivity and viscosity enhancement were shown to correlate with specific surface area.
48 For both CNTnf and GNPNf, the variations in density and specific heat with particle
49 loadings do not exhibit any particularly noteworthy behavior with the mixture properties
50 coinciding with volume-averages [27, 45–47].

51 Recent studies that have specifically focused on theoretical, physics-based models of
52 nanofluids with an eye towards heat transfer share many similarities. The use of a similarity
53 variable to combine spatial coordinates as in the original work of Blasius [38] and the ensuing
54 non-dimensionalized equations describing the boundary layer is a standard mathematical
55 formulation. This is the general outline of the approach taken in this manuscript and its
56 antecedents [11–13]. In our previous and current work, we apply a perturbation analysis in
57 order to determine the thermophysical properties and the boundary layer solutions. In a
58 recent model for hybrid nanofluids containing two different nanoparticle additives [48], the
59 model development proceeds via similarity variable transform and solution of the boundary
60 layer equations, but utilizes explicit models for the calculation of thermophysical properties
61 as functions of particle concentration and solves the governing equations as functions thereof.
62 The approach of ref. 48 thus offers greater control of the input properties, but is significantly
63 more computationally intensive. Other recent models also examine boundary layer flow,
64 but with added physics. Some examples include explicit treatment of thermophoresis [49–

52], magnetohydrodynamics [51–54], flow in porous media [51, 54–56], natural convection
 66 (buoyant or gravitational force) [49, 50, 53, 55–57], and extension to three-dimensional
 67 boundary layer models [52, 58].

68 1.1. Perturbative description of mixture properties

69 The model methodology is given in detail in ref. 11 and 12. The nanofluid is treated
 70 as a base fluid, with properties identified by subscript f , to which a quantity of particles,
 71 subscript p , has been added. Analysis follows a continuum description of the resulting
 72 mixture, as in ref. 5, except that the thermophoresis effect, which has been found to be
 73 relatively unimportant in ref. 5, is not considered.

74 The local volume fraction of particles within the nanofluid mixture is identified as ϕ . We
 75 take $\phi \ll 1$, which is consistent with experimental nanofluid mixtures [59].

76 For an arbitrary material property of the nanofluid, z , we differentiate the property with
 77 respect to the bulk particle concentration, ϕ_∞ , about zero concentration and normalize by
 78 the base fluid property,

$$z^* = \frac{z}{z_f} = 1 + \phi \left(\frac{dz^*}{d\phi_\infty} \right)_{\phi=0} + \mathcal{O}(\phi_\infty^2) \quad (1)$$

79 In the preceding formulation, Φ is the dimensionless volume fraction, ϕ/ϕ_∞ . To simplify
 80 notation, we will indicate derivatives of material properties with respect to the bulk particle
 81 concentration, $\frac{dz^*}{d\phi_\infty}$, with “prime” notation, *e.g.*,

$$z^* = 1 + \phi (z^*)'_{\phi=0} + \mathcal{O}(\phi_\infty^2) \quad (2)$$

82 The properties of the nanofluid required for the analysis of fluid flow and heat transfer
 83 are: the density, ρ ; specific heat capacity, c ; viscosity, μ ; and thermal conductivity, k .
 84 We assume that particle diffusion in the base fluid is governed by Brownian diffusion [5]
 85 and independent of particle concentration, ϕ . Brownian motion is random movement of the
 86 nanoparticles within the base fluid due to molecular collisions. The binary diffusion constant
 87 for the nanoparticles in the base fluid is assigned variable D with dimensionality of area per
 88 time. Calculating D from the Einstein-Stoke’s equation,

$$D = \frac{k_B T}{3\pi\mu d_p} \quad (3)$$

89 where k_B is Boltzmann's constant, T is the fluid temperature, and d_p is the particle diameter.
 90 For typical conditions, $T \approx 300K$, $D \approx (5 \times 10^{-19} m^3/s) / d_p$.

91 *1.2. Boundary layer velocity, concentration, and temperature profiles*

92 In the entrance region of the microchannels, we draw an analogy to boundary layer flow
 93 over a flat plate. Spatial coordinates are defined from the leading edge of the plate. The
 94 abscissa has zero value at the leading edge and increases with distance parallel to the plate's
 95 surface. The ordinate is zero at the plate's surface and measures distance perpendicular to
 96 the surface. Free stream properties are identified with subscript ∞ ; values at the wall by
 97 0. Far from the wall are the free-stream flow velocity, U_∞ , and fluid temperature, T_∞ . Due
 98 to the no-slip boundary condition, the velocity at the wall is zero and the velocity grows
 99 in magnitude as one moves perpendicular to the wall until reaching the free stream value.
 100 Similarly, should the wall temperature differ from that of the flow, as in a heat transfer
 101 application, then there will be a temperature difference relative to the free stream which
 102 decreases as one moves away from the wall. The height above the wall or plate at which the
 103 velocity reaches the free stream value is the momentum boundary layer thickness; the analog
 104 for temperature is the thermal boundary layer thickness. A comprehensive treatment of this
 105 subject is provided by Schlichting in ref. 60. A schematic representation of the velocity and
 106 temperature profiles above the wall is shown in figure 1.

107 Of ultimate interest is determination of the heat transfer and fluid friction as functions
 108 of the nanofluid particle type and concentration relative to the base fluid.

109 We let u be the fluid velocity parallel to the wall and v is the fluid velocity perpendicular
 110 to the wall. The local nanoparticle volume fraction is ϕ and local temperature is T .

111 Surface heat transfer, q , in the boundary layer is due to the temperature gradient at the
 112 wall and enthalpy transport by the nanoparticles, *i.e.*

$$q_0 = - \left(k \frac{\partial T}{\partial y} \right)_0 + (j_p h_p)_0 \quad (4)$$

113 where the mass flux of particles is j_p , mass per area per time, and the unit enthalpy of the
 114 particles, energy per mass, is denoted by h_p .

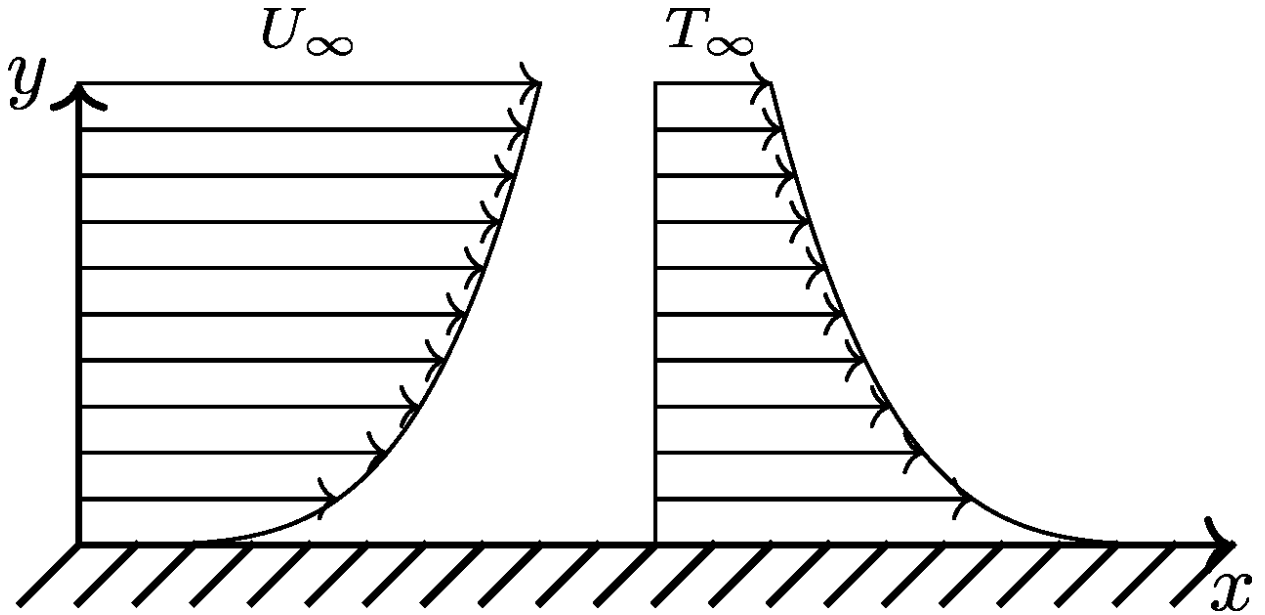


Figure 1: Schematic representation of velocity and temperature profiles for flow over a plate or wall.

115 Utilizing a Fickian diffusion model [61],

$$j_p = - \left(\rho_p D \frac{\partial \phi}{\partial y} \right)_0 + \mathcal{O}(\phi^2) \quad (5)$$

116 Thus, the heat transfer rate is expressed as

$$q_0 = - \left(k \frac{\partial T}{\partial y} \right)_0 - \left(\rho_p D \frac{\partial \phi}{\partial y} h_p \right)_0 \quad (6)$$

117 The surface shear stress, τ_0 , force per area, is defined as the product of the fluid viscosity,
 118 μ , and the streamwise velocity gradient at the wall, *i.e.*,

$$\tau_0 = \mu \left(\frac{\partial u}{\partial y} \right)_{y=0} \quad (7)$$

119 We combine the preceding expressions for heat transfer and mass diffusion with the
 120 continuity (equation 8), momentum (equation 9), energy (equation 10), and mass diffusion
 121 (equation 11) equations for the two-dimensional boundary layer. Momentum is considered
 122 in the streamwise direction with zero pressure gradient. Non-dimensionalization of the
 123 equations is performed as in as in ref. 11. Solution of the continuity, momentum, thermal
 124 energy, and mass diffusion equations must be carried out for variable nanofluid properties

125 (as in equation 2) for the velocity, particle concentration, and temperature profiles in the
 126 steady, two-dimensional boundary layer of laminar flow over a flat plate.

127 Three dimensionless parameters for the transport in the base fluid are also introduced
 128 here: The Prandtl number, Pr , relates viscous to thermal diffusion and is equivalent to $\mu c/k$.
 129 The Schmidt number, Sc , relates viscous to mass diffusion and is equivalent to $\mu/\rho D$. The
 130 Reynolds number, Re , relates inertia to viscosity and is equivalent to $U_\infty L_c \rho/\mu$ where L_c is a
 131 characteristic streamwise length scale and the free stream velocity, U_∞ , is the characteristic
 132 velocity associated with this problem.

133 Spatial coordinates x and y are normalized by L_c to obtain x^* and y^* , respectively. We
 134 let u^* be the fluid velocity parallel to the wall normalized by the free stream velocity, U_∞ ,
 135 such that the free stream value is $u^* = 1$. Similarly, v^* is the fluid velocity perpendicular to
 136 the wall normalized by the free stream velocity. The local volume fraction is normalized by
 137 the bulk concentration $\Phi = \phi/\phi_\infty$. The temperature field is described non-dimensionally by
 138 $\theta = (T - T_\infty)/(T_0 - T_\infty)$.

$$\frac{\partial \rho^* u^*}{\partial x^*} + \frac{\partial \rho^* v^*}{\partial y^*} = 0 \quad (8)$$

$$\rho^* \left(u^* \frac{\partial u^*}{\partial x^*} + v^* \frac{\partial u^*}{\partial y^*} \right) = \frac{1}{Re} \frac{\partial}{\partial y^*} \left(\mu^* \frac{\partial u^*}{\partial y^*} \right) \quad (9)$$

$$\rho^* c^* u^* \frac{\partial \theta}{\partial x^*} + \rho^* c^* v^* \frac{\partial \theta}{\partial y^*} = \frac{1}{Re Pr_f} \frac{\partial}{\partial y^*} \left(k^* \frac{\partial \theta}{\partial y^*} \right) + \frac{\phi_\infty}{Re Sc_f} \frac{\partial}{\partial y^*} \left(\rho_p^* D^* \frac{\partial \Phi}{\partial y^*} c_p^* \theta \right) \quad (10)$$

$$u^* \frac{\partial \Phi}{\partial x^*} + v^* \frac{\partial \Phi}{\partial y^*} = \frac{1}{Re Sc_f} \frac{\partial}{\partial y^*} \left(D^* \frac{\partial \Phi}{\partial y^*} \right) \quad (11)$$

The preceding equations are subject to the non-dimensional boundary conditions:

$$y^* = 0 : u^* = 0, \theta = 1, \Phi = \phi_0/\phi_\infty$$

$$y^* = \infty : u^* = 1, \theta = 0, \Phi = 1$$

139 Physically, the boundary conditions have the following meanings: At the plate or wall,
 140 $y = y^* = 0$: There, owing to the no-slip boundary condition, the velocity is zero, *i.e.*
 141 $u = u^* = 0$. The temperature at the wall is described by T_0 . Normalization of temperature

142 with $\theta = (T - T_\infty) / (T_0 - T_\infty)$ requires $\theta = 1$ at the wall. For Φ , we either define the
 143 concentration at the wall (ϕ_0), as is useful in the case of particle removal or injection, or,
 144 alternatively, the slope may be defined. In the previous work describing a zero flux wall
 145 condition, the boundary condition was specified as $\partial\phi/\partial y^* = 0$ at $y^* = 0$ [11]. The value ϕ_0
 146 is the value of ϕ at the wall, *i.e.* at $y^* = 0$, and is specified as part of the problem description.
 147 We will later examine the three cases of $\phi_0 = \phi_\infty$, a uniform particle distribution, $\phi_0 = 0$,
 148 in which particles are removed at the wall, and $\Phi_0 = 2\phi_\infty$, in which particles are injected at
 149 the wall. The three cases correspond to specifying values at the wall of $\Phi = 1$, $\Phi = 0$, and
 150 $\Phi = 2$, respectively.

151 At infinite distance from the plate or wall, $y = y^* = \infty$: The streamwise velocity is at
 152 its maximum value, the freestream velocity, $u = U_\infty$, $u^* = 1$. The fluid temperature in the
 153 freestream is T_∞ ; the definition of θ fixes this condition as $\theta = 0$. Finally, the normalized
 154 particle concentration in the freestream must also be unity by definition as Φ is the ratio of
 155 the local concentration, ϕ to the freestream concentration ϕ_∞ .

156 By perturbative expansion, our variables take the form

$$G = G_0 + \phi_\infty G_1 + \mathcal{O}(\phi_\infty^2) \quad (12)$$

157 where G is any one of f (introduced below), u^* , v^* , Φ , or θ .

158 Spatial coordinates x^* and y^* are recast into the Blasius similarity variable $\eta = y^* \sqrt{Re/x^*}$
 159 and stream function $\psi^* = f(\eta) \sqrt{x^*/Re}$, velocities u^* and v^* become encoded in a single
 160 function, f , where $u^* = df/d\eta$ and $v^* = [(\eta(df/d\eta) - f) / (2\sqrt{x^*Re})]$ [38, 60]. The non-
 161 dimensional form of the Blasius similarity variable utilized here is obtained by substituting
 162 the characteristic length scale L_c into the dimensional form $\eta = y \sqrt{U_\infty/(\nu x)}$, where ν is
 163 equivalent to μ/ρ . We need only make the substitutions $x = x^* L_c$ and $y = y^* L_c$ and utilize
 164 the aforementioned definition of the Reynolds number, $Re = U_\infty L_c \rho / \mu$.

165 With our variables perturbative form, following equation 12, we arrive at a set of differ-
 166 ential equations and boundary conditions to characterize our system. Derivatives of f , Φ ,
 167 and θ are identified with “prime” notation where derivatives are taken with respect to the
 168 similarity variable, η . The problems for f_0 and θ_0 ($\phi_\infty = 0$) are well-known from the work

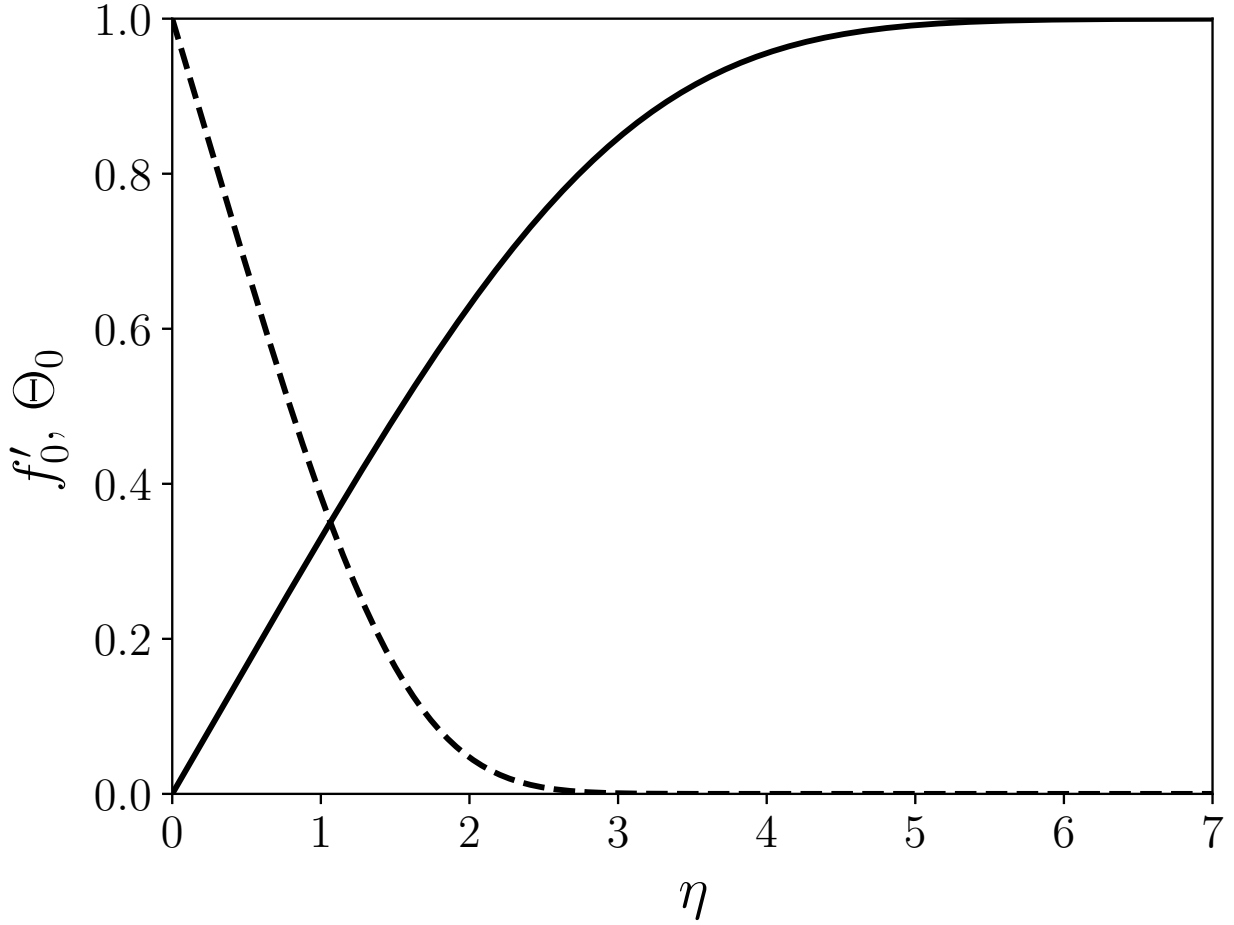


Figure 2: The zeroth-order solutions to the momentum ($f'_0(\eta)$) and thermal boundary layers ($\theta_0(\eta, Pr_f)$) for the base fluid with $Pr_f = 7.0$. $f'_0(\eta)$: —; $\theta_0(\eta, Pr_f)$: - - -

169 of Blasius [38] and Pohlhausen [39], respectively. Detailed treatments of both problems are
 170 compiled in ref. 60.

171 The solutions to the Blasius momentum boundary layer [$f'_0(\eta)$] and Pohlhausen thermal
 172 boundary layer [$\theta_0(\eta, Pr_f)$] are depicted in figure 2.

173 The concentration problem for Φ is necessarily a first-order perturbation as particle
 174 concentration is absent in the base fluid. The problems for f_1 and θ_1 define the perturbative
 175 influence on f_0 and θ_0 via the freestream particle concentration ϕ_∞ with the functional form
 176 given in equation 12.

177 Observing the results for the base fluid in figure 2, it is possible to observe the boundary

178 layer thickness in the absence of nanoparticles. The function f'_0 , equivalent to u_0^* , asymptotes
 179 by $\eta \gtrsim 5$ and the thermal boundary layer is somewhat thinner as θ_0 asymptotes by $\eta \lesssim 3$.

$$f_1''' + \frac{(f_0 f_1'' + f_0'' f_1)}{2} = \frac{f_0 f_0'' \Phi_1}{2} \left[(\mu^*)'_{\phi=0} - (\rho^*)'_{\phi=0} \right] + f_0'' \Phi_1' (\mu^*)'_{\phi=0} \quad (13)$$

$$f_1(0) = f_1'(0) = f_1(\infty) = 0$$

$$\theta_1'' + \frac{Pr_f (f_0 \theta_1' + f_1 \theta_0')}{2} = -\theta_0'' \Phi_1 \left[(k^*)'_{\phi=0} - (\rho^* c^*)'_{\phi=0} \right] - \theta_0' \Phi_1' (k^*)'_{\phi=0} - \frac{\rho_p^* c_p^* D^*}{Sc_f} (\Phi_1' \theta_0)' \quad (14)$$

$$\theta_1(0) = \theta_1(\infty) = 0$$

$$\Phi_1'' + \frac{Sc_f f_0 \Phi_1'}{2} = 0 \quad (15)$$

$$\Phi_1(0) = \Phi_0, \Phi_1(\infty) = 1$$

185 The resulting fundamental equations resemble those of the compressible boundary layer
 186 because of the dependence of flow quantities on the volume fraction, which is determined by
 187 its diffusion equation [11, 12]. It is worth observing that assuming the same binary diffusion
 188 constant and particle diameter across nanofluids, the solution to equation 15 will be identical
 189 and independent of the particle properties discussed below and recorded in table 1.

190 2. Particle and nanofluid properties

191 To examine and predict the properties of CNTNf and GNPNf, material properties of
 192 representative nanofluids were either taken directly from experimental observations (“exp”)
 193 [14, 36] or approximated from the properties of the nanoparticles via mixture theory (“mix”)
 194 [11]. In the case of experimental measurements, density, heat capacity, thermal conductivity,
 195 or viscosity of a prepared nanofluid is measured. Mixture theory estimates the nanofluid
 196 properties by a volume-weighted average of the property of interest for the base fluid and
 197 for the nanoparticle. The CNTNf values reported by ref. 14 are for multi-walled CNT
 198 (MWCNT) particles in water at 1% volume concentration. The experimental values of ref.
 199 14 are used as they represent a complete set of properties for a particular CNTNf preparation

200 rather than pick individual properties from varying sources. Comparing the values of ref. 14
 201 with others reported in literature, there is a strongly non-linear effect reported for the effect
 202 on thermal conductivity: If the real effect of nanoparticle addition to the base fluid on a
 203 property of interest is (strongly) non-linear, then this modeling approach is not strictly valid.
 204 However, based on the history of perturbation analysis and linearization via Taylor series
 205 expansion, by appropriately bounding the maximum nanoparticle concentration, it should
 206 be possible to define a region in which the model can offer useful predictions. Examination
 207 of the modeling results with the goal of determining the conditions for which the model is
 208 valid is discussed in greater detail, below, in section 3.4.

209 The value utilized in this work is $(k^*)'_{\phi=0} = 2.5$ taken from data at 1% volume particle
 210 concentration. Recent work [40] on experimental measurements of MWCNT-water nanoflu-
 211 ids shows a wide range of possible values of $(k^*)'_{\phi=0}$ (as defined via equation 2) ranging from
 212 approximately $(k^*)'_{\phi=0} \approx 7$ at $\phi = 0.0048$ up to $(k^*)'_{\phi=0} \approx 45$ at $\phi = 0.0005$. The lower value
 213 at higher concentration is consistent with earlier findings ($(k^*)'_{\phi=0} \approx 8$ at $\phi = 0.006$ [22])
 214 and the higher value at lower concentration is trend-wise consistent with other experiments
 215 as well ($(k^*)'_{\phi=0} \approx 60$ at $\phi = 0.001$ [62]).

216 Similarly, for the relationship of nanofluid viscosity to nanoparticle concentration for
 217 MWCNT-water mixtures, there are experimental data in literature which suggest non-linear
 218 behaviour in the very low particle-loading conditions. Data recently presented in ref. 32
 219 show that for $\phi \lesssim 0.001$ the nominal value of $(\mu^*)'_{\phi=0} \approx 200$, which agrees with the values
 220 reported by ref. 14 and utilized in this work. For particle loadings an order of magnitude
 221 lower, however, ref. 32 reports data which suggest $(\mu^*)'_{\phi=0} \gtrsim 500$.

222 The GNPNf values for $(\mu^*)'_{\phi=0}$ and $(k^*)'_{\phi=0}$ as reported by ref. 36 are consistent with
 223 results of other experiments, such as those of ref. 44 and reported in recent reviews [27].
 224 The non-dimensionalized values describing the thermophysical properties of the nanofluids
 225 as a function of particle concentration are summarized in table 1.

Table 1: Nanoparticle effects on nanofluid properties

	CNTNf [14]	GNPNf [36]
$(\rho^*)'_{\phi=0}$	0.4 (exp)	1.3 (mix)
$(\rho^*c^*)'_{\phi=0}$	-1.62 (exp)	-0.62 (mix)
$(\mu^*)'_{\phi=0}$	200 (exp)	350 (exp)
$(k^*)'_{\phi=0}$	2.5 (exp)	210 (exp)
$(\mu^*)'_{\phi=0} - (\rho^*)'_{\phi=0}$	199.6	348.7
$(k^*)'_{\phi=0} - (\rho^*c^*)'_{\phi=0}$	4.12	210.62

226 3. Discussion and Results

227 Numerical solution of the governing equations was accomplished by sequentially solving
 228 for f_0 , f_1 , Φ_1 , θ_0 , and θ_1 . Unknown boundary conditions at the wall were iteratively de-
 229 termined by casting method and the differential equations were solved utilizing the LSODE
 230 routine [63] as implemented in OCTAVE [64].

231 Nanoparticle effects are not limited to augmenting the molecular transport coefficients.
 232 In convective flows, both the perturbation temperature and velocity (and concentration)
 233 profiles are altered owing to convective transport effects. The net effect in the perturbation
 234 problem is revealed by the competition between molecular transport and convective trans-
 235 port, represented by the last two rows in Table 1, $(\mu^*)'_{\phi=0} - (\rho^*)'_{\phi=0}$ and $(k^*)'_{\phi=0} - (\rho^*c^*)'_{\phi=0}$.
 236 The convective effects are also interpreted as inertia effects as they are reflected by the rate
 237 of change or adjustment process to be balanced by molecular transport.

238 Examining the governing equations derived for velocity, particle concentration, and tem-
 239 perature, some observations can be made about the behavior of the nanofluid in comparison
 240 with the base fluid. Examining equation 13, the nanofluid effects appear on the right side in
 241 the term $\left[(\mu^*)'_{\phi=0} - (\rho^*)'_{\phi=0} \right]$. For the temperature profile, equation 14, the direct nanofluid
 242 effects appear on the right side; the inhomogeneous, convective effect of $\frac{1}{2}\theta'_0 f_1 Pr_f$ is indirect.

243 Numerical solution of the various cases utilizes water as the base fluid, for which $\nu =$
 244 $\mu/\rho \approx 1 \times 10^{-6} m^2/s$. As in ref. 12, the Schmidt number is taken as 2×10^4 , corresponding
 245 to a nanoparticle diameter $\mathcal{O}(10 \text{ nm})$.

246 The CNT particles are given as having diameters between 20 and 30 nm and lengths

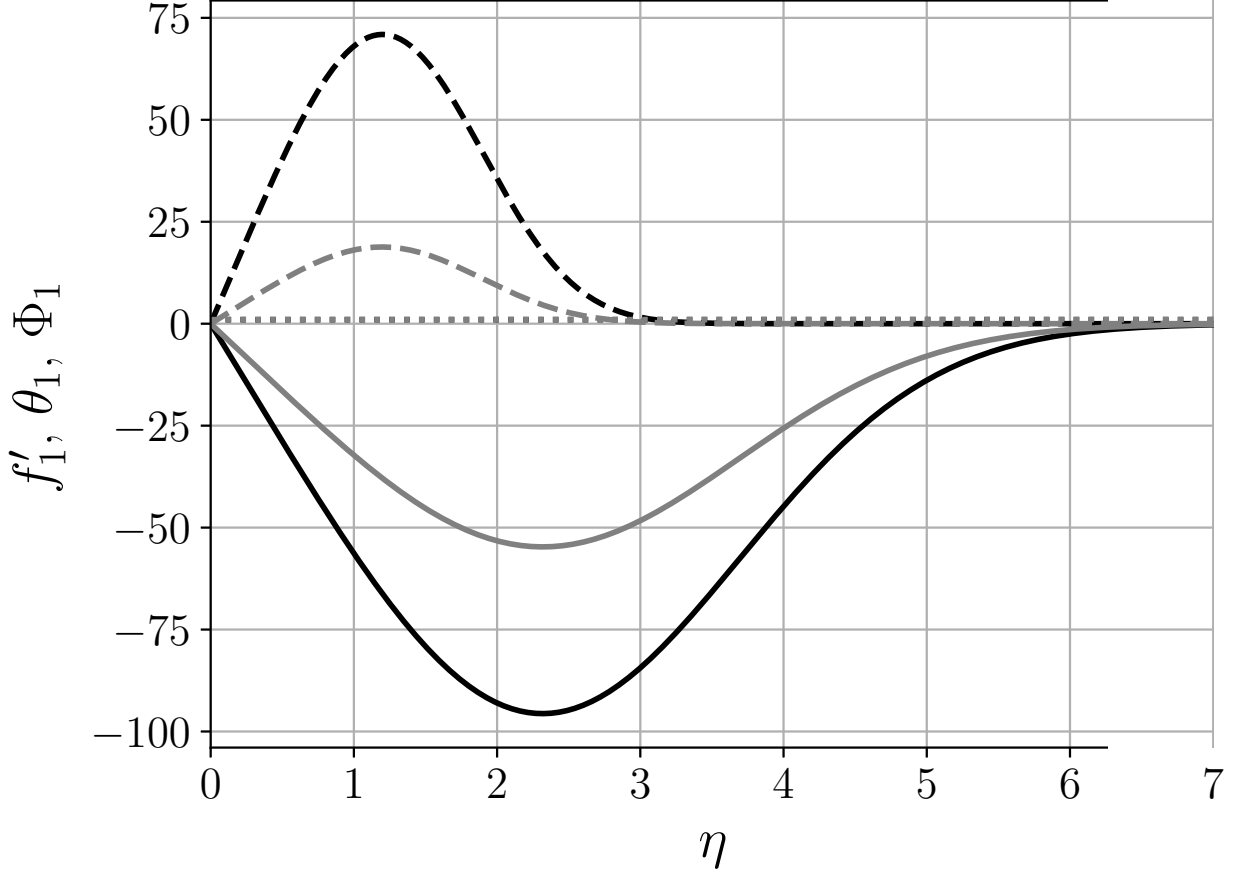


Figure 3: The first-order perturbation functions with zero particle flux at the wall ($\Phi(0, Sc_f) = 1$), $Pr_f = 7.0$, $Sc_f = 2 \times 10^4$. $f'_1(\eta)$: GNPNf: —, CNTNf: —; $\theta_1(\eta, Pr_f)$: GNPNf: ---, CNTNf: ---; $\Phi_1(\eta, Sc_f)$: GNPNf: ·····, CNTNf: ····· (identical solutions ($\Phi_1 = 1$) $\forall \eta$)

247 (thickness) between 1 and 5 nm [14]. The GNP of are similarly described as having a
 248 thickness of 1 to 5 nm [36].

249 3.1. Solid wall (zero particle flux)

250 The volume concentration, for a solid wall, has a zero flux wall boundary condition
 251 ($\Phi'_1(0) = 0 \leftrightarrow \Phi_0 = 1$). In the absence of sources (or sinks), it thus remains constant at the
 252 free stream value [11, 12]. Expressed in terms of solution to equation 15, $\Phi_1 = 1 \forall \eta$.

253 The profiles f'_1 , θ_1 (and ($\Phi_1 = 1$) $\forall \eta$) for CNTNf and GNPNf are shown in figures 3 and
 254 4.

255 For both nanofluids, we observe that the function f'_1 reaches its asymptote at $\eta \lesssim 6$,
 256 which is greater than the value for f'_0 (figure 2). Thus, the perturbative effect is present

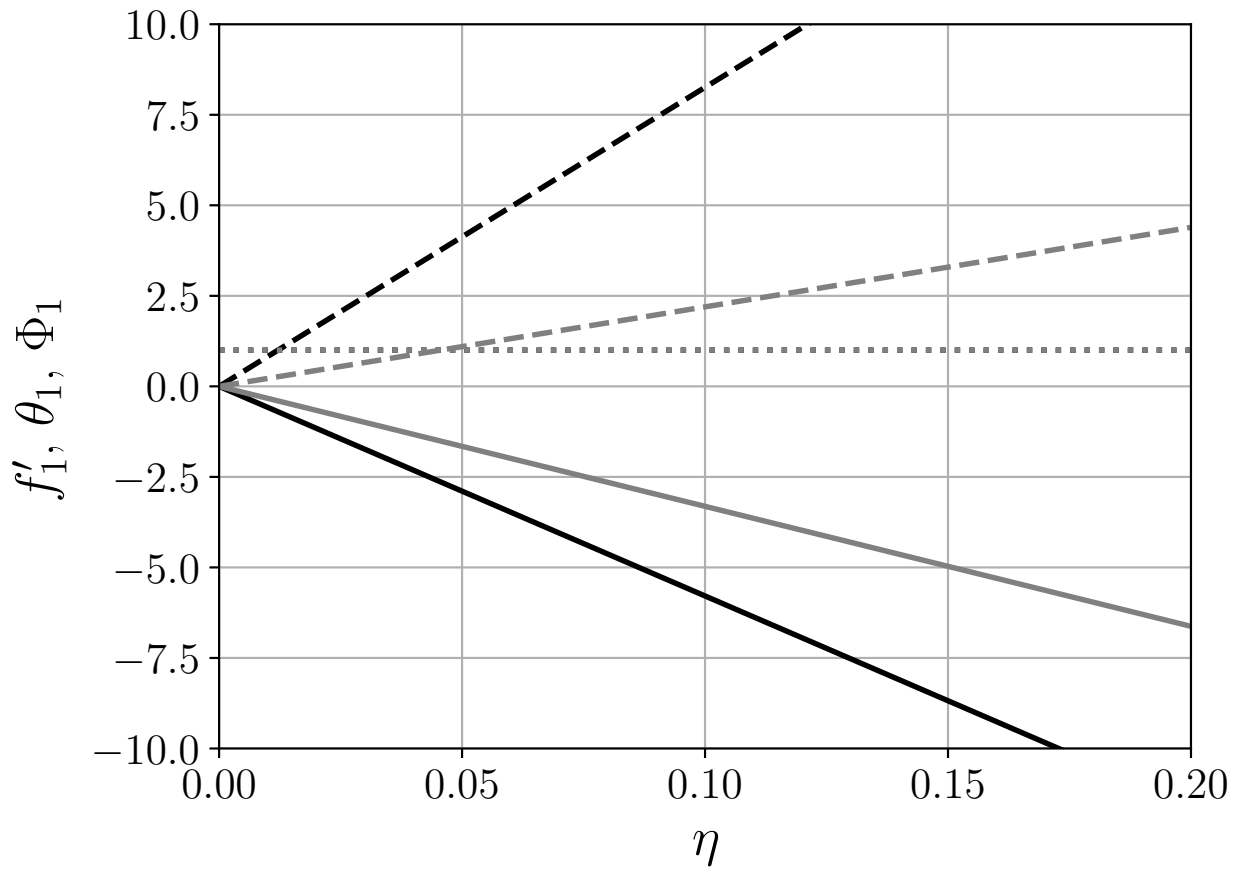


Figure 4: The first-order perturbation functions with zero particle flux at the wall ($\Phi(0, Sc_f) = 1$), $Pr_f = 7.0$, $Sc_f = 2 \times 10^4$, detail view. $f'_1(\eta)$: GNPNf: —, CNTNf: —; $\theta_1(\eta, Pr_f)$: GNPNf: ---, CNTNf: ---; $\Phi_1(\eta, Sc_f)$: GNPNf: ·····, CNTNf: ····· (identical solutions ($\Phi_1 = 1$) $\forall \eta$)

257 beyond the boundary layer thickness of the base fluid, leading to an overall thickening of
 258 the boundary layer.

259 Owing to the large viscosity effect relative to inertia for both nanofluids, (Table 1),
 260 the factor $(\mu^*)'_{\phi=0} - (\rho^*)'_{\phi=0} > 0$, in which case the velocity profile is stretched because of
 261 viscous diffusion; as $(f'_0 \geq 0) \forall \eta$ and $(f'_1 \leq 0) \forall \eta$, the overall effect is to not only thicken
 262 the boundary layer layer, but to reduce the value of $u^* = u_0^* + \phi_\infty u_1^* + \mathcal{O}(\phi_\infty^2)$ throughout
 263 the domain.

264 The magnitude of the effect on the momentum boundary layer and streamwise velocity
 265 is more severe for GNPNf, reaching a negative maximum larger than that of the CNTNf
 266 because of the stronger viscosity effect. This is in contrast to previous studies [11–13] of
 267 alumina and gold nanofluids where $(\mu^*)'_{\phi=0} - (\rho^*)'_{\phi=0} < 0$. The first-order nanofluid effect
 268 on the temperature profile is also shown in figure 3 and 4. As with momentum, the GNPNf
 269 shows stronger modification of the temperature profile than CNTNf because of the stronger
 270 convective transport effect $((k^*)'_{\phi=0} - (\rho^* c^*)'_{\phi=0})$, table 1). A visual comparison of figures
 271 2 and 3, however, indicates that there is negligible impact on the thermal boundary layer
 272 thickness in both nanofluid cases.

273 In the first-order perturbation theory, the nanofluid effect is defined, and embedded in,
 274 the dimensionless slope times the volume fraction. Referring back to ref. 11, in this linear
 275 perturbation model, the normalized shear stress, τ^* , and surface heat transfer, q^* reduce to
 276 the following:

$$\tau^* = 1 + \phi_\infty \left[(\mu^*)'_{\phi=0} + f_1''(0) / f_0''(0) \right] \equiv 1 + \phi_\infty (\tau^*)'_{\phi=0} \quad (16)$$

$$q^* = 1 + \phi_\infty \left[(k^*)'_{\phi=0} + \theta_1''(0) / \theta_0''(0) \right] \equiv 1 + \phi_\infty (q^*)'_{\phi=0} \quad (17)$$

277 The surface heat transfer and shear stress results are then expressed in terms of the
 278 slopes: for CNTNf, $(\tau^*)'_{\phi=0} = 100.2$, $(q^*)'_{\phi=0} = -31.54$. For GNPNf, $(\tau^*)'_{\phi=0} = 175.7$,
 279 $(q^*)'_{\phi=0} = 82.10$.

280 As may be observed from the preceding values and in figure 5, for both CNTNf and
 281 GNPNf, the increase in heat transfer relative to the increase in shear stress is less than unity,

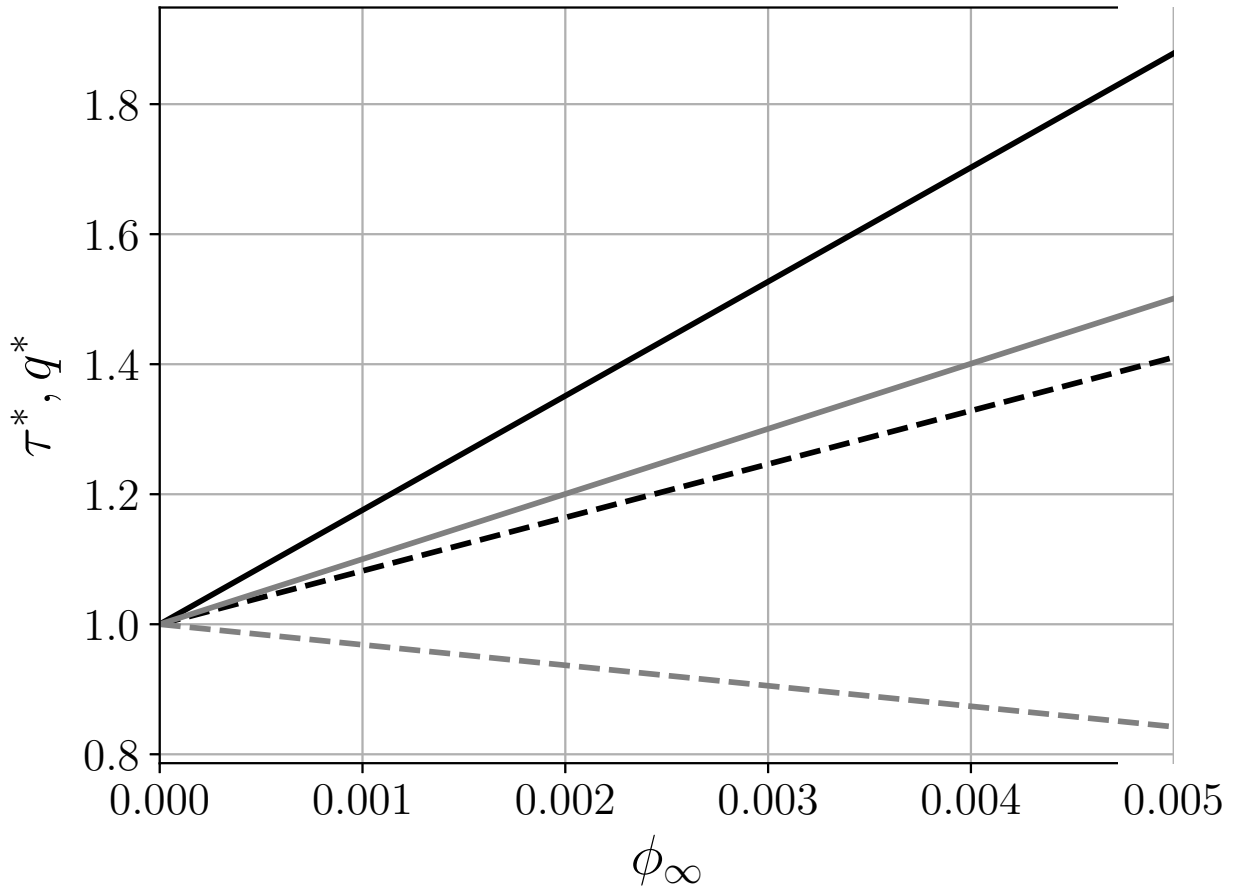


Figure 5: Heat transfer enhancement and shear stress rise as functions of volume fraction with zero particle flux at the wall ($\Phi(0, Sc_f) = 1$), $Pr_f = 7.0$, $Sc_f = 2 \times 10^4$. τ^* : GNPNf: ———, CNTNf: ———; q^* : GNPNf: — — —, CNTNf: — — —

282 *i.e.* $q^*/\tau^* < 1$. Further, it is noteworthy that $(q^*)'_{\phi=0} < 0$ for CNTNf. In previous studies
 283 of alumina and gold nanofluids [11, 12], all the slopes are positive, *i.e.* such nanofluids
 284 increase the surface heat transfer and shear stress to the various degrees dictated by the
 285 respective thermophysical properties. It is important to explicitly note that the magnitude
 286 of the negative slope will necessarily impose a bound on the applicability of the model:
 287 values of $q^* < 0$ or $\tau^* < 0$ are non-physical and accordingly restrict the range in which
 288 this model may be valid. Through simple manipulation of equation 17, it is clear that the
 289 material properties of the CNTNf given in table 1 must be collectively invalid for $\phi_{cr} \gtrsim$
 290 $\left(-[(q^*)'_{\phi=0}]^{-1}\right) = 0.0274$ and that linear scaling of the material properties about zero
 291 concentration of particles is not representative for CNTNf with particle concentrations in
 292 the vicinity of ϕ_{cr} .

293 There are some data available in the literature with which results may be compared:
 294 A study of a CNTNf consisting of MWCNT in water at $\phi \leq 0.01$ found that for fluid
 295 flow undergoing transition from laminar to turbulent, “transition flow”, at $Re_D = 2000$,
 296 $8 \lesssim (q^*)'_{\phi=0} \lesssim 15$ between about 20 and 70 tube diameters [15]. However, the data measured
 297 closest to the entrance region, at approximately 10 diameters, showed much less and even
 298 negative values, $-5 \lesssim (q^*)'_{\phi=0} \lesssim 3$. GNP were mixed into a hybrid water-ethylene glycol
 299 base fluid in ref. 45. Experimental measures on mixtures with $\phi \leq 0.005$ taken in an
 300 automotive radiator showed $50 \lesssim (q^*)'_{\phi=0} \lesssim 300$, which is consistent with the results reported
 301 here, but also showed a general trend of the value of $(q^*)'_{\phi=0}$ decreasing with increasing
 302 Reynolds number. Also from ref. 45, measured pressure loss suggests $100 \lesssim (\tau^*)'_{\phi=0} \lesssim 800$,
 303 trending downward with increasing Reynolds number and showing some dependence on
 304 ϕ , with increased particle concentration showing lower pressure loss at the same Reynolds
 305 number.

306 3.2. Porous wall (non-zero particle flux)

307 It is now worth examining CNTNf and GNPNf in the case of porous walls where the
 308 particle concentration may differ from that in the bulk fluid. The case of particle removal,
 309 with zero particle concentration at the wall, $\Phi(0, Sc_f) = 0$, is considered first and the

Table 2: Nanofluid transport results

Case	$(\tau^*)'_{\phi=0}$	$(q^*)'_{\phi=0}$
GNPNf, $\Phi(0, Sc_f) = 0$	-174.00	270.90
GNPNf, $\Phi(0, Sc_f) = 1$	175.65	82.10
GNPNf, $\Phi(0, Sc_f) = 2$	525.30	-106.69
CNTNf, $\Phi(0, Sc_f) = 0$	-99.60	-36.50
CNTNf, $\Phi(0, Sc_f) = 1$	100.20	-31.54
CNTNf, $\Phi(0, Sc_f) = 2$	300.00	-26.58

310 perturbation functions are shown in figures 6 and 7. It is only on very close examination
 311 of figure 6 that any difference to figure 3 is observable; comparison of figures 7 and 4,
 312 however, makes clear the impact of the particle concentration on the perturbative functions
 313 at the wall. The values of $(\tau^*)'_{\phi=0}$ for both CNTNf and GNPNf decrease and change sign,
 314 indicating absolute reduction in the nanofluid shear stress relative to the base fluid and to
 315 the solid wall case for low particle loadings. Heat transfer is nearly unchanged for CNTNf
 316 with particle removal at the wall, but is greatly enhanced for GNPNf. The predicted impact
 317 on shear stress and heat transfer is shown in figure 8. These predictions for the case of
 318 particle removal at the wall must be taken with a grain of salt, however, as the negative
 319 values of $(\tau^*)'_{\phi=0}$ lead to values of $\phi_{cr} \lesssim 0.0101$ for CNTNf and $\phi_{cr} \lesssim 0.0058$ for GNPNf.

320 Turning to particle injection, results are generated for a particle concentration at the wall
 321 twice that in the bulk fluid, $\Phi(0, Sc_f) = 2$. The associated perturbation functions are shown
 322 in figure 9 and in detail in figure 10. Here, shear stress increases and heat transfer decreases
 323 for both nanofluids relative to the solid wall, with the heat transfer slopes becoming negative,
 324 *i.e.* $(q^*)'_{\phi=0} < 0$, for both fluids. Shear stress and heat transfer as a function of particle
 325 loading for the case of wall injection are shown in figure 11. The upper restrictions on the
 326 valid range of the model, for this case become $\phi_{cr} \lesssim 0.0377$ for CNTNf and $\phi_{cr} \lesssim 0.0094$ for
 327 GNPNf.

328 The computed values of $(\tau^*)'_{\phi=0}$ and $(q^*)'_{\phi=0}$ for CNTNf and GNPNf for each of the three
 329 cases of particle concentration at the wall are provided in table 2.

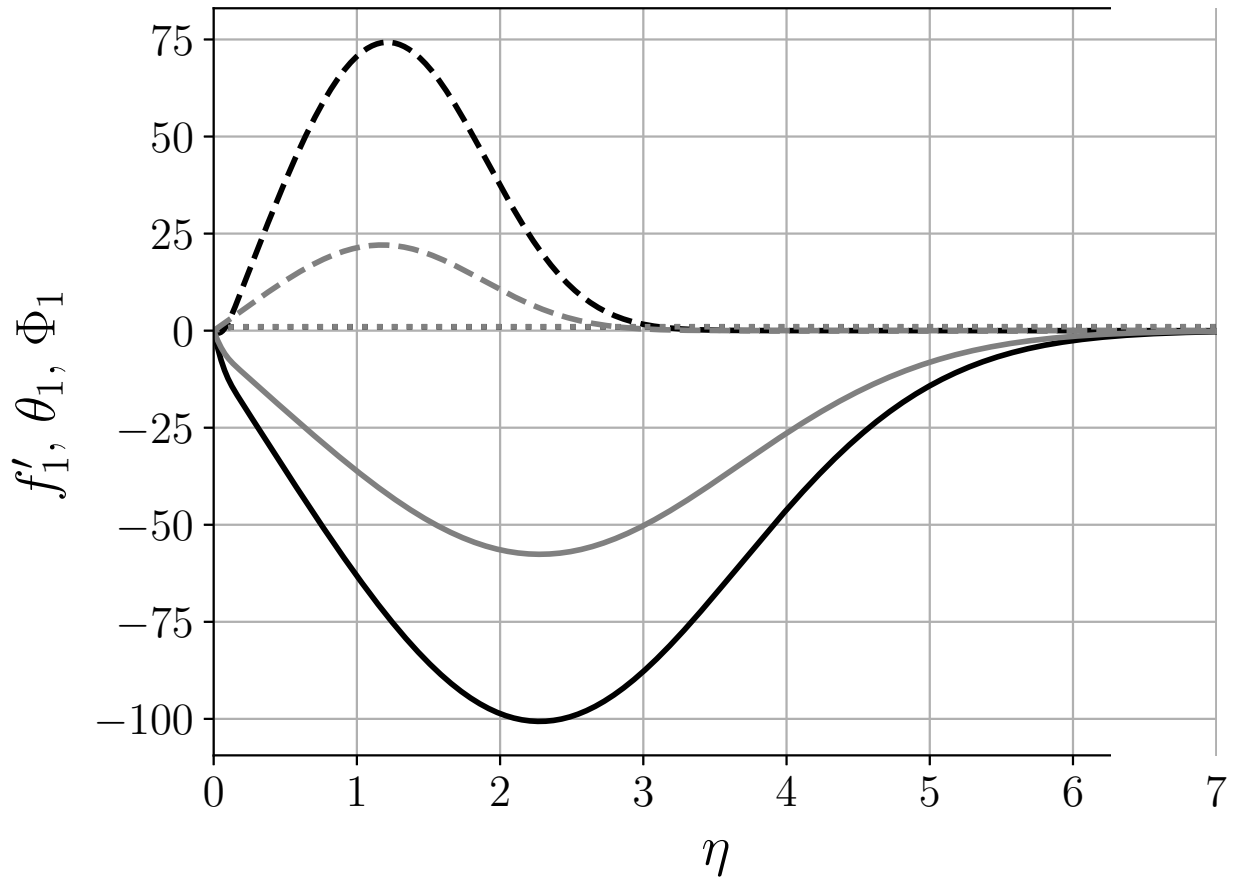


Figure 6: The first-order perturbation functions with particle removal (zero concentration) at the wall ($\Phi(0, Sc_f) = 0$), $Pr_f = 7.0$, $Sc_f = 2 \times 10^4$. $f'_1(\eta)$: GNPNf: —, CNTNf: —; $\theta_1(\eta, Pr_f)$: GNPNf: ---, CNTNf: ---; $\Phi_1(\eta, Sc_f)$: GNPNf: ·····, CNTNf: ····· (identical solutions)

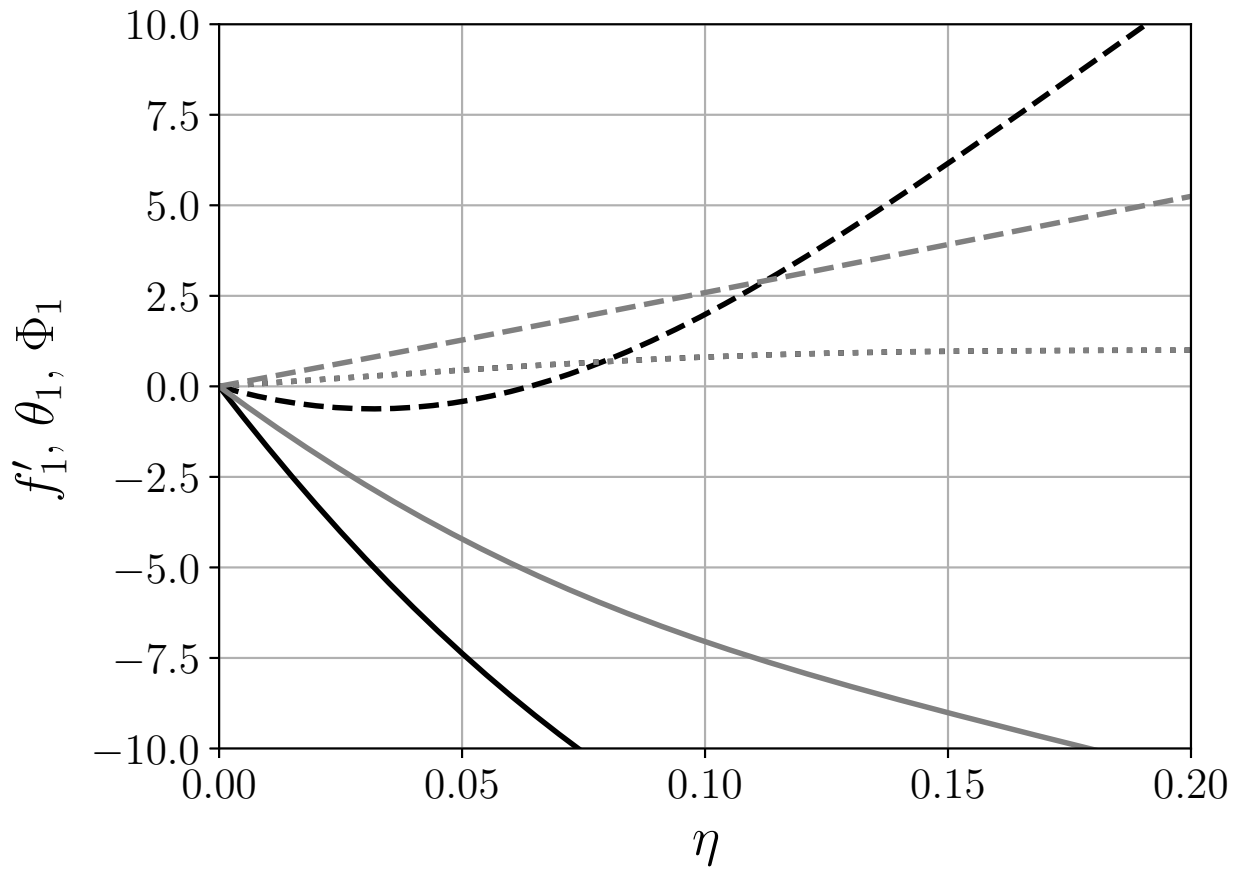


Figure 7: The first-order perturbation functions with particle removal (zero concentration) at the wall ($\Phi(0, Sc_f) = 0$), $Pr_f = 7.0$, $Sc_f = 2 \times 10^4$, detail view. $f'_1(\eta)$: GNPnf: —, CNTNf: —; $\theta_1(\eta, Pr_f)$: GNPnf: ---, CNTNf: ---; $\Phi_1(\eta, Sc_f)$: GNPnf: ·····, CNTNf: ····· (identical solutions)

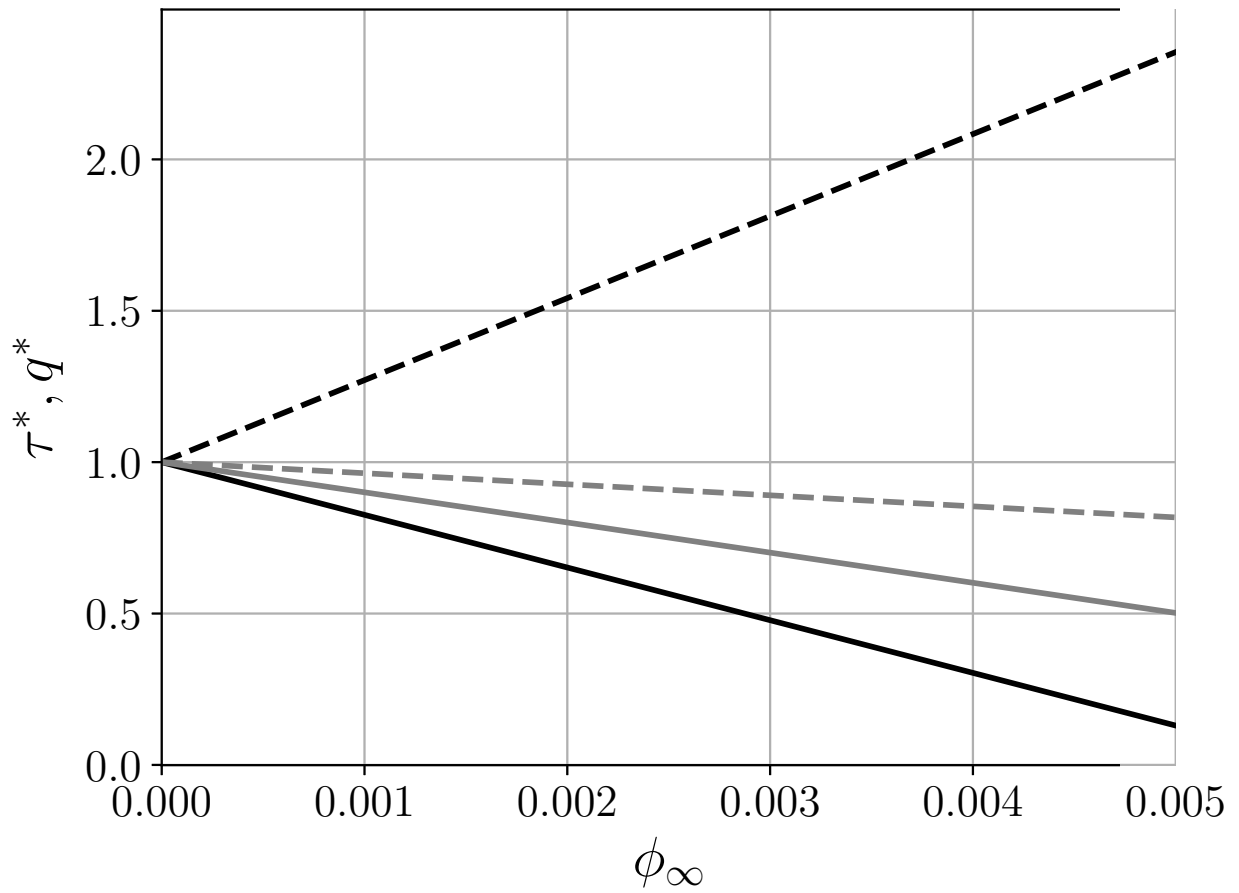


Figure 8: Heat transfer enhancement and shear stress rise as functions of volume fraction with particle removal (zero concentration) at the wall ($\Phi(0, Sc_f) = 0$), $Pr_f = 7.0$, $Sc_f = 2 \times 10^4$. τ^* : GNPNf: —, CNTNf: —; q^* : GNPNf: ---, CNTNf: ---

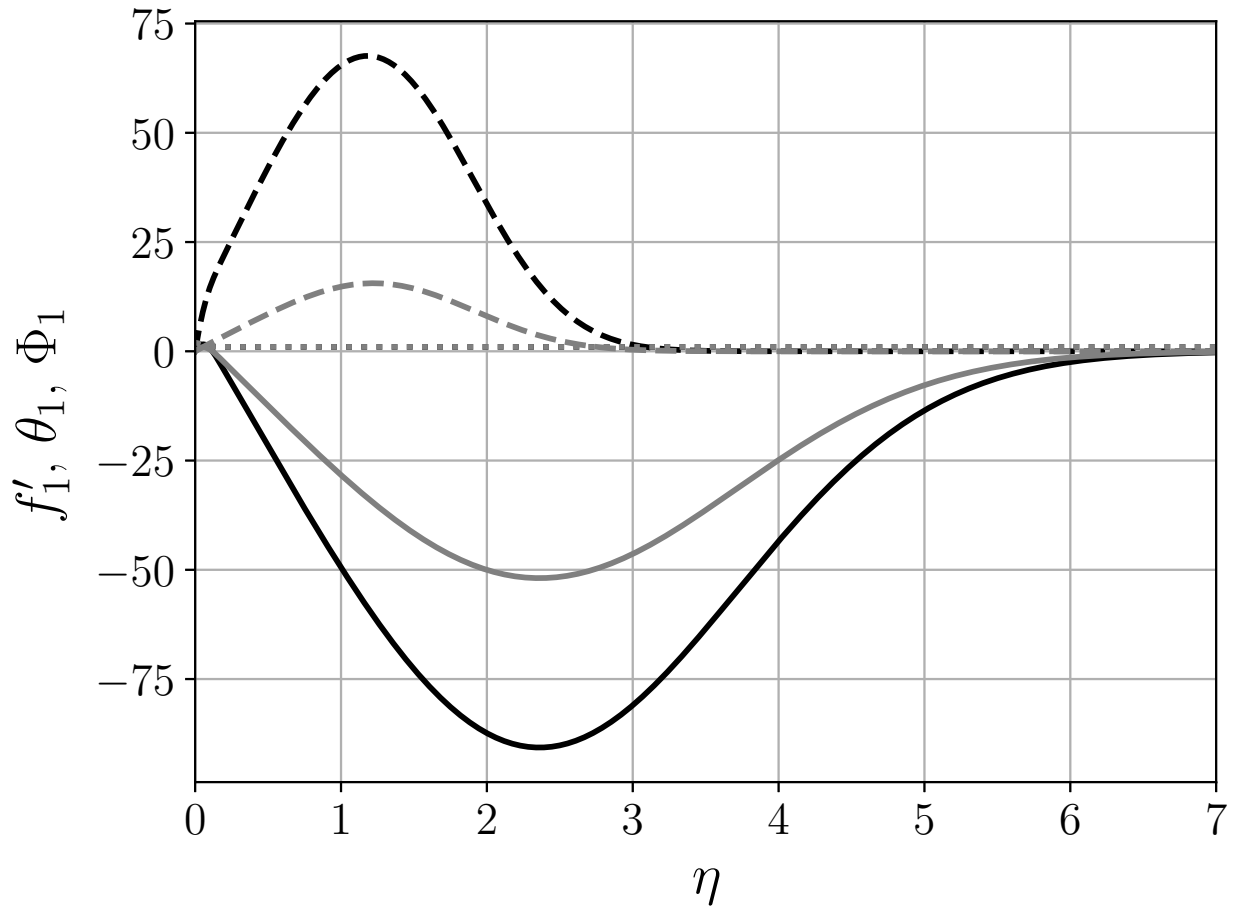


Figure 9: The first-order perturbation functions with particle injection at the wall ($\Phi(0, Sc_f) = 2$), $Pr_f = 7.0$, $Sc_f = 2 \times 10^4$. $f'_1(\eta)$: GNPNf: —, CNTNf: —; $\theta_1(\eta, Pr_f)$: GNPNf: ---, CNTNf: ---; $\Phi_1(\eta, Sc_f)$: GNPNf: ·····, CNTNf: ····· (identical solutions)

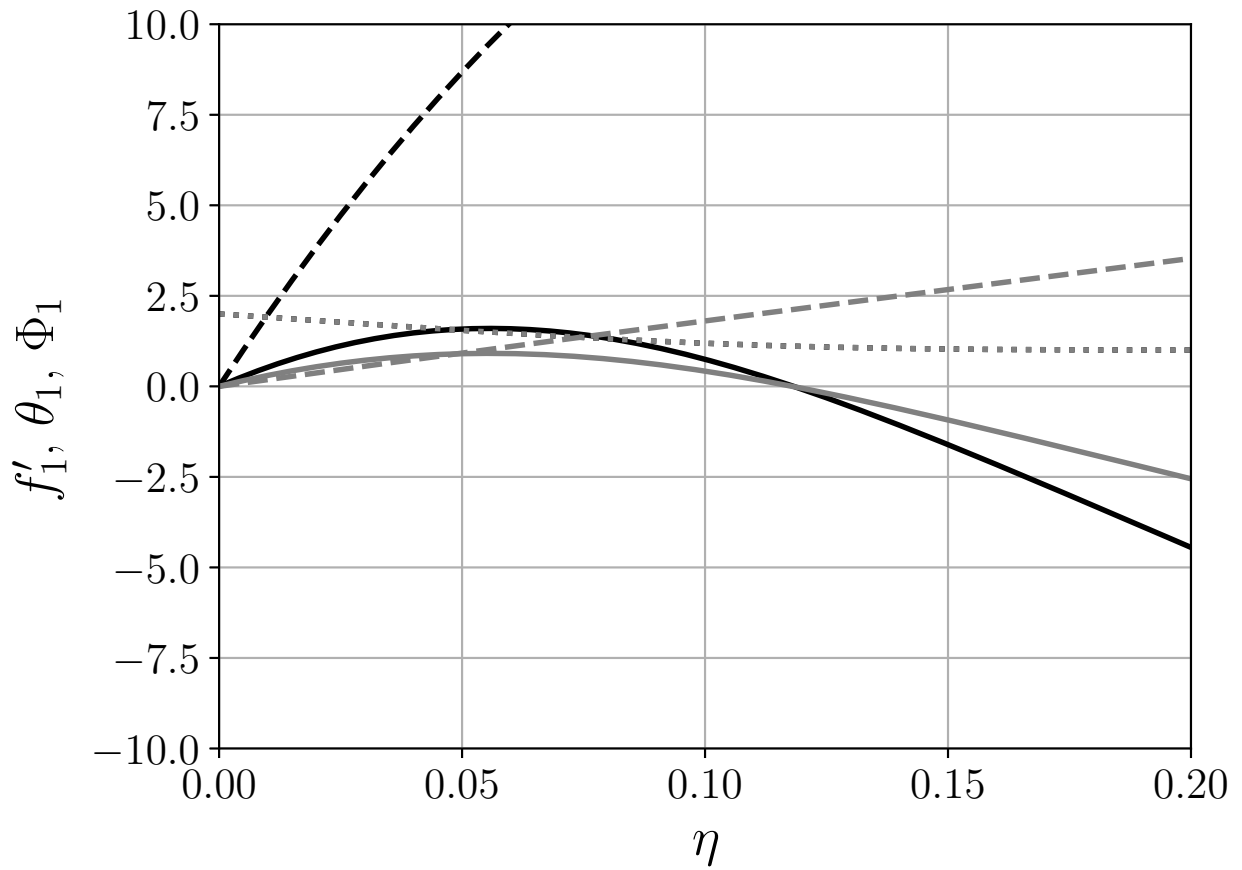


Figure 10: The first-order perturbation functions with particle injection at the wall ($\Phi(0, Sc_f) = 2$), $Pr_f = 7.0$, $Sc_f = 2 \times 10^4$, detail view. $f'_1(\eta)$: GNPNf: —, CNTNf: —; $\theta_1(\eta, Pr_f)$: GNPNf: ---, CNTNf: ---; $\Phi_1(\eta, Sc_f)$: GNPNf: ·····, CNTNf: ····· (identical solutions)

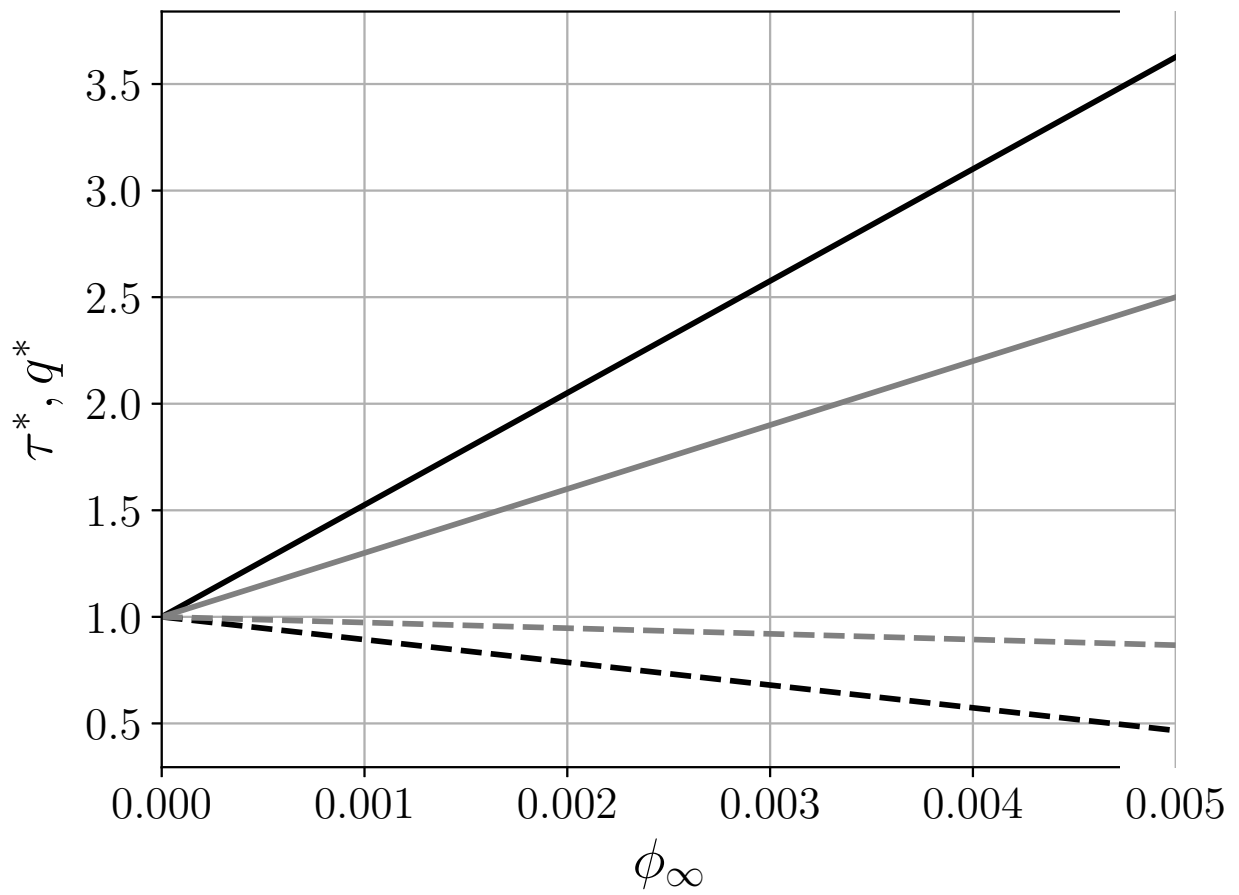


Figure 11: Heat transfer enhancement and shear stress rise as functions of volume fraction with particle injection at the wall ($\Phi(0, Sc_f) = 2$), $Pr_f = 7.0$, $Sc_f = 2 \times 10^4$. τ^* : GNPnf: ———, CNTnf: ———; q^* : GNPnf: - - -, CNTnf: - - -

330 *3.3. Comparison with metallic nanofluids*

331 It is worth briefly discussing a comparison of these carbon particle nanofluids, CNTNf and
332 GNPNf, with alumina and gold nanofluids investigated previously with the same modeling
333 approach [11, 12]. As mentioned above, interest in nanofluids is concentrated on applications
334 to improve heat transfer. A nanofluid whose increase in heat transfer is proportionally
335 outstripped by the increase in pumping power, characterized by shear stress, $q^*/\tau^* < 1$, is
336 not going to provide the desired benefit in most cases as heat transfer could be increased at
337 lower cost by increasing the pumping rate, rather than adding nanoparticles.

338 A general analysis for competition between increased shear stress and increased heat
339 transfer was made in ref. 15 in which it was determined that the requirement for a practical
340 nanofluid, *i.e.* one in which the benefits outweigh the costs, is $(\mu^*)'_{\phi=0} \leq 4(k^*)'_{\phi=0}$.

341 Comparisons of CNTNf and GNPNf with the alumina and gold nanoparticle simulations
342 of ref. 11 and ref. 12 for the solid wall and porous walls cases of particle removal and
343 injections are provided, respectively, in figures 12, 13, and 14.

344 Examining the comparisons at each wall condition, it is quite explicit that for the solid
345 wall, figure 12, the metallic nanoparticles offer near-unity ratios of heat transfer to shear
346 stress enhancement, with alumina particles out-performing gold and achieving greater gains
347 in heat transfer than in shear stress. The carbon nanofluids show significantly poorer per-
348 formance and exhibit proportionally larger impacts on the nanofluid properties relative to
349 metallic particles.

350 Turning to the case of particle removal at the wall, figure 13, both carbon nanofluids
351 show a positive, enhancing behavior, but for GNPNf $\phi_{cr} \lesssim 0.0058$. When compared with
352 experimental volume fractions of metallic particles, this is extremely low, *cf.* ref. 59, but
353 it is seemingly acceptable for the range of volume fractions found in carbon and graphene
354 particle nanofluids, *cf.* ref. 40.

355 Finally, in the case of particle injection, figure 14, the results are visually similar to the
356 solid wall case. The ratio of heat transfer to shear stress enhancement is less than unity for
357 all materials, but again the metallic nanoparticles and carbon nanoparticles are distinctly
358 separated from each other.

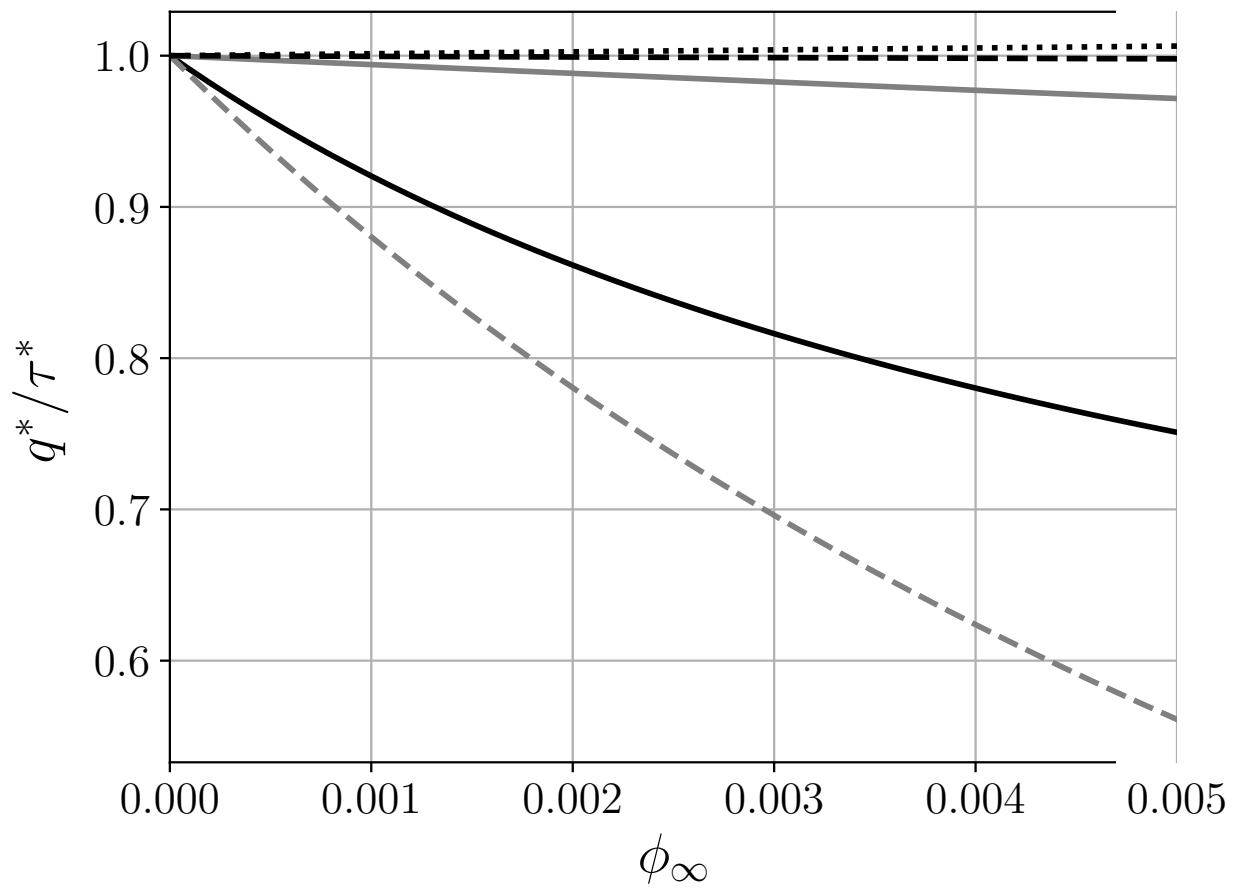


Figure 12: Heat transfer enhancement and shear stress rise as functions of volume fraction with zero particle flux at the wall ($\Phi(0, Sc_f) = 1$), $Pr_f = 7.0$, $Sc_f = 2 \times 10^4$. GNPnf: —, CNTNf: ---, Alumina:, Gold (mix): —, Gold (MD): ---

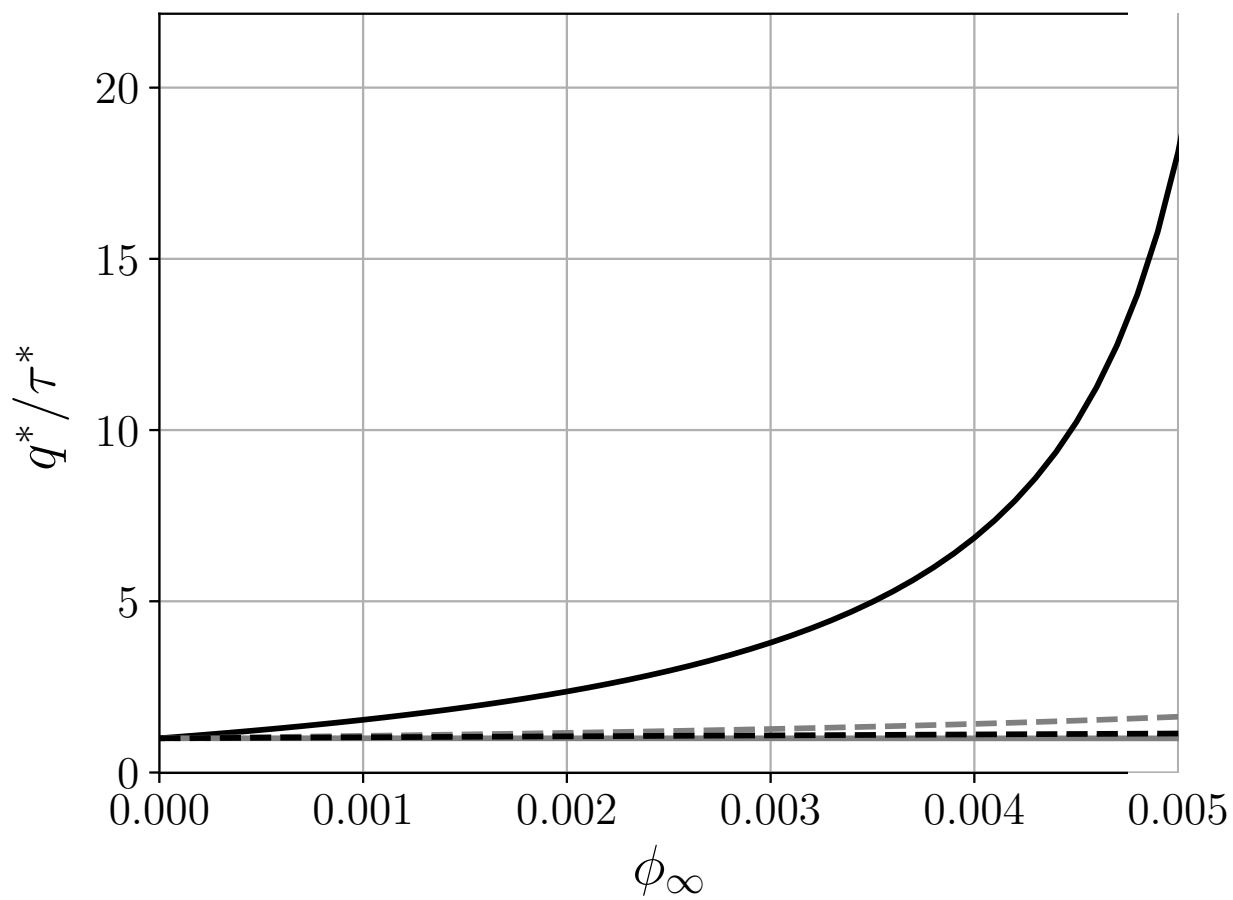


Figure 13: Heat transfer enhancement and shear stress rise as functions of volume fraction with zero particle concentration at the wall ($\Phi(0, Sc_f) = 0$), $Pr_f = 7.0$, $Sc_f = 2 \times 10^4$. GNPnf: —, CNTNf: ---, Alumina: ·····, Gold (mix): —, Gold (MD): ---

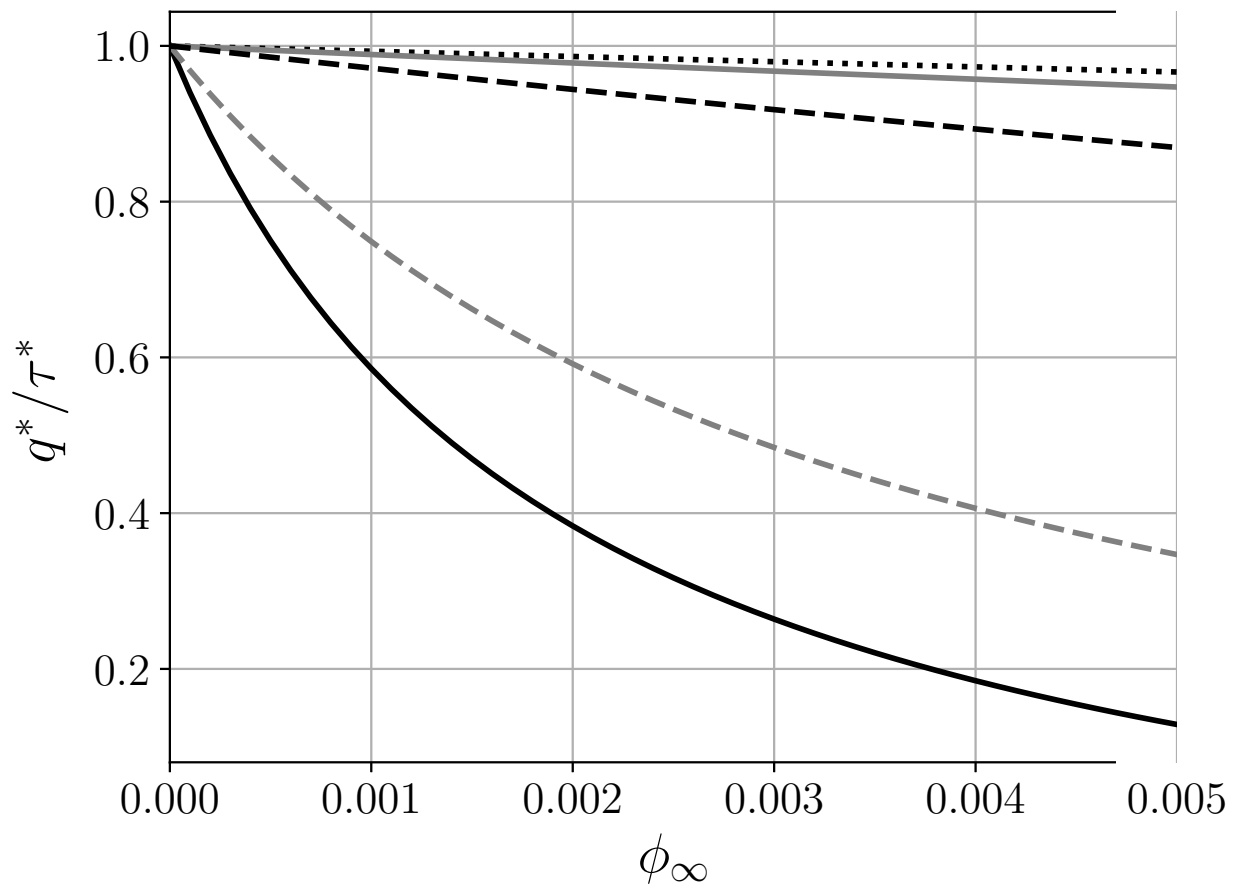


Figure 14: Heat transfer enhancement and shear stress rise as functions of volume fraction with particle injection at the wall ($\Phi(0, Sc_f) = 2$), $Pr_f = 7.0$, $Sc_f = 2 \times 10^4$. GNPNf: —, CNTNf: ---, Alumina: ·····, Gold (mix): —, Gold (MD): ---

359 3.4. Model limitations

360 In each of the cases examined, the value of ϕ_{cr} has been determined to identify a loose
361 upper bound on the range for which the model utilized here may be appropriate. The lower
362 values of ϕ_{cr} for GNPNf versus CNTNf are a direct effect of the more dramatic impact
363 on transport in the nanofluid effected by GNP in comparison with CNT. The values of
364 $(\mu^*)'_{\phi=0}$ and $(k^*)'_{\phi=0}$ are both greater for GNPNf than CNTNf, necessarily leading to a
365 breakdown in linearity at lower values of ϕ . It is thus appropriate to also discuss the
366 uncertainty in the value of $(k^*)'_{\phi=0}$ taken for CNTNf. Recalling the reported values in
367 literature, there is a trend of proportionally greater enhancement in thermal conductivity at
368 lower concentrations. Including this trend would have the effect of introducing feedback into
369 our current linearization where as the input value of $(k^*)'_{\phi=0}$ is adjusted up to correspond to
370 an experimental measurement at a lower particle concentration, ϕ , the value of ϕ_{cr} would also
371 fall. The International Nanofluid Property Benchmark Exercise (INPBE) [59] demonstrated
372 good agreement among over thirty research groups in measured thermal conductivity of
373 nanofluids and good agreement to effective medium theory [65] to model the nanofluid
374 thermal conductivity as a function of particle loading. The experimental data measured
375 in ref. 40 and presented in ref. 27 stand in contrast to other publications showing good
376 agreement to approximations per equation 2 for viscosity and thermal conductivity [15, 45,
377 66].

378 4. Conclusion

379 The present studies indicate that both CNTNf and GNPNf incur very large increases in
380 shear stress at the wall relative to alumina and gold nanofluids; similarly for surface heat
381 transfer for GNPNf but the relative increase is only about half as great as the relative increase
382 in the shear stress. Of exception is the surface heat transfer for CNTNf, which shows anti-
383 enhancement behaviour, principally due to the interaction of the convective effects of the
384 strongly viscous dominated momentum problem. More accurate representations of nanofluid
385 thermophysical properties as functions of the volume fraction and fluid temperature are
386 suggested. Specifically, additional experimental measurements of the properties of CNTNf

387 and GNPNf and associated heat transfer and shear stress over a broad range of particle
388 loadings are desired.

389 References

- 390 [1] Choi S.U.S. and Eastman J.A. *Enhancing thermal conductivity of fluids with nanoparticles*. In *ASME*
391 *International Mechanical Engineering Congress & Exposition*. 1995.
- 392 [2] Das S.K., Choi S.U.S., and Patel H.E. *Heat transfer in nanofluids—a review*. *Heat Transfer Engineering*,
393 27(10):3–19, 2006. doi:10.1080/01457630600904593.
- 394 [3] Murshed S.M.S. and de Castro C.A.N., eds. *Nanofluids : synthesis, properties, and applications*. Nova
395 Science Publishers, Inc, New York, New York, 2014. ISBN 9781633216778.
- 396 [4] Murshed S.M.S. and de Castro C.A.N. *Nanofluids as advanced coolants*. In *Green Solvents I*, pp.
397 397–415. Springer Netherlands, 2012. doi:10.1007/978-94-007-1712-1_14.
- 398 [5] Buongiorno J. *Convective transport in nanofluids*. *Journal of Heat Transfer*, 128(3):240–250, 2006.
399 doi:10.1115/1.2150834.
- 400 [6] Liu J.T.C. *On the anomalous laminar heat transfer intensification in developing region of nanofluid*
401 *flow in channels or tubes*. *Proceedings of the Royal Society A: Mathematical, Physical and Engineering*
402 *Sciences*, 468(2144):2383–2398, 2012. doi:10.1098/rspa.2011.0671.
- 403 [7] Trisaksri V. and Wongwises S. *Critical review of heat transfer characteristics of nanofluids*. *Renewable*
404 *and Sustainable Energy Reviews*, 11(3):512–523, 2007. doi:10.1016/j.rser.2005.01.010.
- 405 [8] Corcione M. *Empirical correlating equations for predicting the effective thermal conductivity and*
406 *dynamic viscosity of nanofluids*. *Energy Conversion and Management*, 52(1):789–793, 2011. doi:
407 10.1016/j.enconman.2010.06.072.
- 408 [9] Murshed S.S., de Castro C.N., Lourenço M., Lopes M., and Santos F. *A review of boiling and convective*
409 *heat transfer with nanofluids*. *Renewable and Sustainable Energy Reviews*, 15(5):2342–2354, 2011. doi:
410 10.1016/j.rser.2011.02.016.
- 411 [10] Wong K.V. and Leon O.D. *Applications of nanofluids: Current and future*. *Advances in Mechanical*
412 *Engineering*, 2:519659, 2010. doi:10.1155/2010/519659.
- 413 [11] Liu J.T.C., Fuller M.E., Wu K.L., Czulak A., Kithes A.G., and Felten C.J. *Nanofluid flow and heat*
414 *transfer in boundary layers at small nanoparticle volume fraction: Zero nanoparticle flux at solid wall*.
415 *Archives of Mechanics*, 69:75–100, 2017.
- 416 [12] Barbosa De Castilho C.J., Fuller M.E., Sane A., and Liu J.T.C. *Nanofluid flow and heat transfer in*
417 *boundary layers at small nanoparticle volume fraction: Non-zero nanoparticle flux at solid wall*. *Heat*
418 *Transfer Engineering*, 40(9–10):725–737, 2019. doi:10.1080/01457632.2018.1442298.
- 419 [13] Hopper D., Jaganathan D., Orr J.L., Shi J., Simeski F., Yin M., and Liu J.T.C. *Heat transfer*
420 *in nanofluid boundary layer near adiabatic wall*. *Journal of Nanofluids*, 7(6):1297–1302, 2018. doi:
421 10.1166/jon.2018.1551.
- 422 [14] Li Y., Suzuki S., Inagaki T., and Yamauchi N. *Carbon-nanotube nanofluid thermophysical properties*
423 *and heat transfer by natural convection*. *Journal of Physics: Conference Series*, 557:012051, 2014.
424 doi:10.1088/1742-6596/557/1/012051.
- 425 [15] Meyer J., McKrell T., and Grote K. *The influence of multi-walled carbon nanotubes on*
426 *single-phase heat transfer and pressure drop characteristics in the transitional flow regime of*
427 *smooth tubes*. *International Journal of Heat and Mass Transfer*, 58(1-2):597–609, 2013. doi:
428 10.1016/j.ijheatmasstransfer.2012.11.074.
- 429 [16] Amrollahi A., Rashidi A., Lotfi R., Meibodi M.E., and Kashefi K. *Convection heat transfer*
430 *of functionalized MWNT in aqueous fluids in laminar and turbulent flow at the entrance re-*
431 *gion*. *International Communications in Heat and Mass Transfer*, 37(6):717–723, 2010. doi:
432 10.1016/j.icheatmasstransfer.2010.03.003.
- 433 [17] Ding Y., Alias H., Wen D., and Williams R.A. *Heat transfer of aqueous suspensions of carbon nanotubes*
434 *(CNT nanofluids)*. *International Journal of Heat and Mass Transfer*, 49(1-2):240–250, 2006. doi:
435 10.1016/j.ijheatmasstransfer.2005.07.009.

- 436 [18] Garg P., Alvarado J.L., Marsh C., Carlson T.A., Kessler D.A., and Annamalai K. *An experimental*
437 *study on the effect of ultrasonication on viscosity and heat transfer performance of multi-wall carbon*
438 *nanotube-based aqueous nanofluids*. International Journal of Heat and Mass Transfer, 52(21-22):5090–
439 5101, 2009. doi:10.1016/j.ijheatmasstransfer.2009.04.029.
- 440 [19] Kakaç S. and Pramuanjaroenkij A. *Review of convective heat transfer enhancement with*
441 *nanofluids*. International Journal of Heat and Mass Transfer, 52(13-14):3187–3196, 2009. doi:
442 10.1016/j.ijheatmasstransfer.2009.02.006.
- 443 [20] Ko G.H., Heo K., Lee K., Kim D.S., Kim C., Sohn Y., and Choi M. *An experimental study on the*
444 *pressure drop of nanofluids containing carbon nanotubes in a horizontal tube*. International Journal of
445 Heat and Mass Transfer, 50(23-24):4749–4753, 2007. doi:10.1016/j.ijheatmasstransfer.2007.03.029.
- 446 [21] Liu Z.H. and Liao L. *Forced convective flow and heat transfer characteristics of aqueous drag-reducing*
447 *fluid with carbon nanotubes added*. International Journal of Thermal Sciences, 49(12):2331–2338, 2010.
448 doi:10.1016/j.ijthermalsci.2010.08.001.
- 449 [22] Xie H., Lee H., Youn W., and Choi M. *Nanofluids containing multiwalled carbon nanotubes and their*
450 *enhanced thermal conductivities*. Journal of Applied Physics, 94(8):4967, 2003. doi:10.1063/1.1613374.
- 451 [23] Yu W., Xie H., Wang X., and Wang X. *Significant thermal conductivity enhancement for*
452 *nanofluids containing graphene nanosheets*. Physics Letters A, 375(10):1323–1328, 2011. doi:
453 10.1016/j.physleta.2011.01.040.
- 454 [24] Sanukrishna S.S. and Prakash M.J. *Exploiting the potentials of graphene nano-platelets for the devel-*
455 *opment of energy-efficient lubricants for refrigeration systems*. In *Springer Transactions in Civil and*
456 *Environmental Engineering*, pp. 303–312. Springer Singapore, 2020. doi:10.1007/978-981-15-1063-2_24.
- 457 [25] Dalkılıç A.S., Mercan H., Özçelik G., and Wongwises S. *Optimization of the finned double-pipe heat*
458 *exchanger using nanofluids as working fluids*. Journal of Thermal Analysis and Calorimetry, 2020.
459 doi:10.1007/s10973-020-09290-x.
- 460 [26] Vallejo J.P., Calviño U., Freire I., Fernández-Seara J., and Lugo L. *Convective heat transfer in pipe*
461 *flow for glycolated water-based carbon nanofluids. a thorough analysis*. Journal of Molecular Liquids,
462 301:112370, 2020. doi:10.1016/j.molliq.2019.112370.
- 463 [27] Borode A.O., Ahmed N.A., and Olubambi P.A. *A review of heat transfer application of carbon-*
464 *based nanofluid in heat exchangers*. Nano-Structures & Nano-Objects, 20:100394, 2019. doi:
465 10.1016/j.nanoso.2019.100394.
- 466 [28] Sanukrishna S.S., Raju A.V., Krishnan A., Harikrishnan G.H., Amal A., Kumar T.S.K., and Prakash
467 M.J. *Enhancing the thermophysical properties of PAG lubricant using graphene nano-sheets*. Journal
468 of Physics: Conference Series, 1355:012041, 2019. doi:10.1088/1742-6596/1355/1/012041.
- 469 [29] Akbari A., Mohammadian E., Fazel S.A.A., Shanbedi M., Bahreini M., Heidari M., and Ahmadi G.
470 *Comparison between nucleate pool boiling heat transfer of graphene nanoplatelet- and carbon nanotube-*
471 *based aqueous nanofluids*. ACS Omega, 4(21):19183–19192, 2019. doi:10.1021/acsomega.9b02474.
- 472 [30] Borode A.O., Ahmed N.A., and Olubambi P.A. *Application of carbon-based nanofluids in heat ex-*
473 *changers: Current trends*. Journal of Physics: Conference Series, 1378:032061, 2019. doi:10.1088/1742-
474 6596/1378/3/032061.
- 475 [31] Hussien A.A., Abdullah M.Z., Yusop N.M., Al-Kouz W., Mahmoudi E., and Mehrali M. *Heat trans-*
476 *fer and entropy generation abilities of MWCNTs/GNPs hybrid nanofluids in microtubes*. Entropy,
477 21(5):480, 2019. doi:10.3390/e21050480.
- 478 [32] Hamze S., Berrada N., Desforges A., Vigolo B., Maré T., Cabaleiro D., and Estellé P. *Dynamic viscosity*
479 *of purified MWCNT water and water-propylene glycol based nanofluids*. In *1st International Conference*
480 *on Nanofluids (ICNf2019), 2nd European Symposium on Nanofluids (ESNf2019)*, pp. 329–332. 2019.
- 481 [33] Shi D., Guo Z., and Bedford N. *Carbon nanotubes*. In *Nanomaterials and Devices*, pp. 49–82. Elsevier,
482 2015. doi:10.1016/b978-1-4557-7754-9.00003-2.
- 483 [34] Harik V. *Classification of carbon nanotubes*. In *Mechanics of Carbon Nanotubes*, pp. 73–105. Elsevier,
484 2018. doi:10.1016/b978-0-12-811071-3.00004-4.
- 485 [35] de Sousa D.E.S., Scuracchio C.H., de Oliveira Barra G.M., and de Almeida Lucas A. *Expanded graphite*
486 *as a multifunctional filler for polymer nanocomposites*. In *Multifunctionality of Polymer Composites*,

- pp. 245–261. Elsevier, 2015. doi:10.1016/b978-0-323-26434-1.00007-6.
- [36] Ahammed N., Asirvatham L.G., and Wongwises S. *Effect of volume concentration and temperature on viscosity and surface tension of graphene–water nanofluid for heat transfer applications*. Journal of Thermal Analysis and Calorimetry, 123(2):1399–1409, 2016. doi:10.1007/s10973-015-5034-x.
- [37] Wen D. and Ding Y. *Experimental investigation into convective heat transfer of nanofluids at the entrance region under laminar flow conditions*. International Journal of Heat and Mass Transfer, 47(24):5181–5188, 2004. doi:10.1016/j.ijheatmasstransfer.2004.07.012.
- [38] Blasius H. *Grenzschichten in Flüssigkeiten mit kleiner Reibung*. Zeitschrift für Angewandte Mathematik und Physik, (56):1–37, 1908.
- [39] Pohlhausen E. *Der Wärmeaustausch zwischen festen Körpern und Flüssigkeiten mit kleiner Reibung und kleiner Wärmeleitung*. ZAMM - Zeitschrift für Angewandte Mathematik und Mechanik, 1(2):115–121, 1921. doi:10.1002/zamm.19210010205.
- [40] Xing M., Yu J., and Wang R. *Experimental study on the thermal conductivity enhancement of water based nanofluids using different types of carbon nanotubes*. International Journal of Heat and Mass Transfer, 88:609–616, 2015. doi:10.1016/j.ijheatmasstransfer.2015.05.005.
- [41] Chen L., Xie H., Li Y., and Yu W. *Nanofluids containing carbon nanotubes treated by mechanochemical reaction*. Thermochimica Acta, 477(1-2):21–24, 2008. doi:10.1016/j.tca.2008.08.001.
- [42] Phuoc T.X., Massoudi M., and Chen R.H. *Viscosity and thermal conductivity of nanofluids containing multi-walled carbon nanotubes stabilized by chitosan*. International Journal of Thermal Sciences, 50(1):12–18, 2011. doi:10.1016/j.ijthermalsci.2010.09.008.
- [43] Chen L., Xie H., Yu W., and Li Y. *Rheological behaviors of nanofluids containing multi-walled carbon nanotube*. Journal of Dispersion Science and Technology, 32(4):550–554, 2011. doi:10.1080/01932691003757223.
- [44] Mehrali M., Sadeghinezhad E., Latibari S., Kazi S., Mehrali M., Zubir M.N.B.M., and Metselaar H.S. *Investigation of thermal conductivity and rheological properties of nanofluids containing graphene nanoplatelets*. Nanoscale Research Letters, 9(1):15, 2014. doi:10.1186/1556-276x-9-15.
- [45] Selvam C., Lal D.M., and Harish S. *Enhanced heat transfer performance of an automobile radiator with graphene based suspensions*. Applied Thermal Engineering, 123:50–60, 2017. doi:10.1016/j.applthermaleng.2017.05.076.
- [46] Askari S., Lotfi R., Seifkordi A., Rashidi A., and Koolivand H. *A novel approach for energy and water conservation in wet cooling towers by using MWNTs and nanoporous graphene nanofluids*. Energy Conversion and Management, 109:10–18, 2016. doi:10.1016/j.enconman.2015.11.053.
- [47] Said Z., Saidur R., Sabiha M., Rahim N., and Anisur M. *Thermophysical properties of single wall carbon nanotubes and its effect on exergy efficiency of a flat plate solar collector*. Solar Energy, 115:757–769, 2015. doi:10.1016/j.solener.2015.02.037.
- [48] Dinarvand S. *Nodal/saddle stagnation-point boundary layer flow of CuO–Ag/water hybrid nanofluid: a novel hybridity model*. Microsystem Technologies, 25(7):2609–2623, 2019. doi:10.1007/s00542-019-04332-3.
- [49] Kuznetsov A. and Nield D. *Natural convective boundary-layer flow of a nanofluid past a vertical plate*. International Journal of Thermal Sciences, 49(2):243–247, 2010. doi:10.1016/j.ijthermalsci.2009.07.015.
- [50] Sheremet M. and Pop I. *Conjugate natural convection in a square porous cavity filled by a nanofluid using Buongiorno’s mathematical model*. International Journal of Heat and Mass Transfer, 79:137–145, 2014. doi:10.1016/j.ijheatmasstransfer.2014.07.092.
- [51] Muhammad T., Alsaedi A., Shehzad S.A., and Hayat T. *A revised model for Darcy-Forchheimer flow of Maxwell nanofluid subject to convective boundary condition*. Chinese Journal of Physics, 55(3):963–976, 2017. doi:10.1016/j.cjph.2017.03.006.
- [52] Hayat T., Muhammad T., Shehzad S., and Alsaedi A. *On three-dimensional boundary layer flow of Sisko nanofluid with magnetic field effects*. Advanced Powder Technology, 27(2):504–512, 2016. doi:10.1016/j.appt.2016.02.002.
- [53] Sheikholeslami M. and Rokni H.B. *Numerical modeling of nanofluid natural convection in a semi annulus in existence of Lorentz force*. Computer Methods in Applied Mechanics and Engineering,

- 538 317:419–430, 2017. doi:10.1016/j.cma.2016.12.028.
- 539 [54] Sheikholeslami M., Shehzad S., Li Z., and Shafee A. *Numerical modeling for alumina nanofluid magne-*
540 *tohydrodynamic convective heat transfer in a permeable medium using Darcy law.* International Journal
541 of Heat and Mass Transfer, 127:614–622, 2018. doi:10.1016/j.ijheatmasstransfer.2018.07.013.
- 542 [55] Kuznetsov A. and Nield D. *The Cheng–Minkowycz problem for natural convective boundary layer flow*
543 *in a porous medium saturated by a nanofluid: A revised model.* International Journal of Heat and Mass
544 Transfer, 65:682–685, 2013. doi:10.1016/j.ijheatmasstransfer.2013.06.054.
- 545 [56] Sheremet M.A., Grosan T., and Pop I. *Free convection in a square cavity filled with a porous medium*
546 *saturated by nanofluid using Tiwari and Das’ nanofluid model.* Transport in Porous Media, 106(3):595–
547 610, 2014. doi:10.1007/s11242-014-0415-3.
- 548 [57] Kuznetsov A. and Nield D. *Natural convective boundary-layer flow of a nanofluid past a verti-*
549 *cal plate: A revised model.* International Journal of Thermal Sciences, 77:126–129, 2014. doi:
550 10.1016/j.ijthermalsci.2013.10.007.
- 551 [58] Muhammad T., Alsaedi A., Hayat T., and Shehzad S.A. *A revised model for Darcy–Forchheimer three-*
552 *dimensional flow of nanofluid subject to convective boundary condition.* Results in Physics, 7:2791–2797,
553 2017. doi:10.1016/j.rinp.2017.07.052.
- 554 [59] Buongiorno J., Venerus D.C., Prabhat N., McKrell T., Townsend J., Christianson R., Tolmachev Y.V.,
555 Keblinski P., wen Hu L., Alvarado J.L., Bang I.C., Bishnoi S.W., Bonetti M., Botz F., Cecere A., Chang
556 Y., Chen G., Chen H., Chung S.J., Chyu M.K., Das S.K., Paola R.D., Ding Y., Dubois F., Dzido G.,
557 Eapen J., Escher W., Funfschilling D., Galand Q., Gao J., Gharagozloo P.E., Goodson K.E., Gutierrez
558 J.G., Hong H., Horton M., Hwang K.S., Iorio C.S., Jang S.P., Jarzebski A.B., Jiang Y., Jin L., Kabelac
559 S., Kamath A., Kedzierski M.A., Kieng L.G., Kim C., Kim J.H., Kim S., Lee S.H., Leong K.C., Manna
560 I., Michel B., Ni R., Patel H.E., Philip J., Poulikakos D., Reynaud C., Savino R., Singh P.K., Song
561 P., Sundararajan T., Timofeeva E., Triticak T., Turanov A.N., Vaerenbergh S.V., Wen D., Witharana
562 S., Yang C., Yeh W.H., Zhao X.Z., and Zhou S.Q. *A benchmark study on the thermal conductivity of*
563 *nanofluids.* Journal of Applied Physics, 106(9):094312, 2009. doi:10.1063/1.3245330.
- 564 [60] Schlichting H. *Boundary-Layer Theory.* McGraw-Hill, sixth edn., 1968.
- 565 [61] Fick A. *Ueber diffusion.* Annalen der Physik und Chemie, 170(1):59–86, 1855. doi:
566 10.1002/andp.18551700105.
- 567 [62] Assael M.J., Metaxa I.N., Arvanitidis J., Christofilos D., and Lioutas C. *Thermal conductivity enhance-*
568 *ment in aqueous suspensions of carbon multi-walled and double-walled nanotubes in the presence of two*
569 *different dispersants.* International Journal of Thermophysics, 26(3):647–664, 2005. doi:10.1007/s10765-
570 005-5569-3.
- 571 [63] Hindmarsh A.C. *Scientific Computing*, chap. ODEPACK, A Systematized Collection of ODE Solvers,
572 pp. 55–64. North-Holland Publishing Company, 1983.
- 573 [64] Eaton J.W., Bateman D., Hauberg S., and Wehbring R. *GNU Octave version 4.0.0 manual: a high-level*
574 *interactive language for numerical computations.* 2015.
- 575 [65] Maxwell J.C. *A treatise on electricity and magnetism*, vol. 2. Clarendon Press, 1881.
- 576 [66] Prasher R., Song D., Wang J., and Phelan P. *Measurements of nanofluid viscosity and its implications*
577 *for thermal applications.* Applied Physics Letters, 89(13):133108, 2006. doi:10.1063/1.2356113.